On the dynamics in a boundary layer

By CUNBIAO LEE and SHIYI CHEN

State Key Laboratory for Turbulence Research and Complex Systems, Peking University, Beijing 100871,China

This paper presents direct comparisons of related visualization and hot film measurement studies of the nonlinear, late stages of transition in a boundary layer. The preceding nonlinear stages of the transition process are well documented in previous studies. Both the visualizations and measurements were performed with controlled disturbance conditions excited by an instability wave in a flat-plate boundary layer. The CS-solitons, the Λ-vortex, the secondary closed vortex and the chain of ring vortices are postulated to be the basic flow structures of the transitional boundary layer. New mechanisms for their formation are also given. Despite somewhat different initial disturbance conditions used in these and previous experiments, the flow structures are found to be practically the same. Our experimental results show new dynamic processes and new flow structures, i.e., the secondary closed vortex, in a transitional boundary layer.

1. Introduction

In 1883 Osborne Reynolds published the outcome of his painstaking flow visualizations at Manchester in the Philosophical Transaction of Royal Society. These showed that the flow transition in a pipe from direct to sinuous (nowadays we would say laminar to turbulent) depended on the Reynolds number. Transition from laminar to turbulent flow is still an important problem in fluid mechanics which has attracted the interest of investigators for more than 100 years. The particular case of boundary layer flow has received the most attention and has been more successfully treated than any other flows. However, despite the success of linearized theories in revealing the nature of the initial stages of boundary layer instability, there remains a deep void in the understanding of the subsequent non-linear behavior and the actual breakdown of the laminar boundary layer. The present state of affairs is such that one must depend on experiments to bridge the gap.

The classic investigations into the mechanics of transition called the K-regime were undertaken at the National Bureau of Standards by Schubauer(1957), Klebanoff & Tidstrom (1957, 1962). The work of Schubauer & Klebanoff (1956) showed transition to be a process involving the formation of turbulent spots, as had been postulated earlier by Emmons (1951). Experimental investigations by Hama & Long(1957), Kovasznay, Komoda and Vasudeva (1962) and Hama & Nautant (1963) utilizing dye techniques in water demonstrated the occurrence of characteristic three-dimensional dye configurations before transition occurs. The three main stages were identified both experimentally and theoretically as (a) receptivity, (b) linear stability, and (c) nonlinear breakdown.

The receptivity problem was clearly formulated for the first time by Morkovin (1969). The idea that the Reynolds number of the pipe-flow transition has to increase when the amplitudes of the disturbances in the incoming flow are attenuated had been suggested by Reynolds more than a century ago and corroborated later in 1905. Loehrke (1975) reviewed the importance of the receptivity problem for understanding transition. A model vibration in the acoustically excited boundary layer for the receptivity problem was shown experimentally and studied by Kachanov et al. (1974a,b), as well as Shapiro (1977). The recent review by Saric gave the more detailed information about the receptivity (2002).

The theoretical studies of the receptivity problem focused on investigating the boundary-layer receptivity to free stream vortices (see Rogler1977, Rogler & Reshotko 1975) and to acoustic waves (Manger 1977, Murdock 1980). Wu (1996) proposed a new mechanism for the generation of Tollmien-Schlichting waves by free-stream turbulence. For definiteness and self-consistency, the mechanism is described using triple-deck formalism. The free-stream turbulence is represented by converting gusts consisting of the so-called vortical and entropy waves of small amplitude. Wu et al. showed that suitable convecting gusts can interact with sound waves in the free-stream to produce a forcing that has the same time and length scales as those of the T-S waves. Wu & Lu (2001) and Wu and Choudhari (2001) also showed that the instability of the incompressible Blasius boundary layer can be significantly modified, and even fundamentally altered, by certain small-amplitude distortions which feature low-speed streaks. The instability of the perturbed flow was shown to be governed by a remarkably simple system described by a Schödinger-like equation with a purely imaginary potential.

The attempts to experimentally investigate boundary-layer stability with respect of three-dimensional disturbances were undertaken in the 1960s by Vasudeva (1967), who used a localized source of instability waves. Later Gaster and Grant (1975) obtained rich information about the development of three-dimensional packets of instability waves in a Blasius boundary layer.

Kachanov (1994) made a direct quantitative comparison of theoretical and experimental data for the dispersion and stability characteristics of three-dimensional instability waves propagating in a flat plate boundary layer. Direct comparison between Direct numerical simulation (DNS) results were compared quantitatively with the K-regime of transition experiments using a DNS scheme based on the spatial simulation model by Bake, Meyer & Rist (2002) and Borodulin, Goponenko, Kachanov, Meyer, Rist, Lian & Lee (2002).

Although the region of nonlinear breakdown has been studied for more than forty years, many aspects remain a mystery. Several new structures have been found in recent years by Kachanov (1994), Bake, Meyer & Rist (2002) and Borodulin, Goponenko, Kachanov, Meyer, Rist, Lian & Lee (2002), Rist & Fasel (1995) and Lee (2000, 2001a,b) with several new scenarios to describe transition by Kachanov (1994) , Reddy, Schmid Braggett & Henningson (1998), Thefethen, Thefethen, Reddy & Driscoll(1993), Waleffe (1995, 1998) and Lee (2000, 2001b).

The structural similarity between transitional and developed boundary layers was first briefly discussed by Blackwelder (1983). Kachanov (1994) discussed the connection between the K-breakdown and the developed turbulence. The flow structures in developed turbulence described by Fukunishi, Sato & Inous (1987) and Thomas & Saric (1981) are very similar to that described by Borodulin and Kachanov (1994). The seminal experimental studies of Kline, Reynolds, Schraub & Runstaller (1967) on the turbulent boundary-layer structure inspired much experimental work (as well as subsequent direct numerical simulations of turbulence), some of which is discussed by Walker, Abbott, Scharnhorst & Weigand (1989), Robinson (1990, 1991a,b). The general character of the readily observable features of boundary layer flows is well established, although an understanding of cause-and-effect relationships has proven elusive. There are two main aspects that dominate the near-wall flow, namely the ‘low speed streaks’ and the ‘bursting’ phenomenon [38]. Along a given area of the wall, streaks may be readily observed during a most of any observation period when a visualization medium, such as dye or hydrogen-bubbles, is introduced into the flow near the surface. The streaks delineate regions where the cross-stream motion converges and the streamwise velocity is in deficit relative to the local mean velocity; sandwiched between the low-speed regions are zones of high-speed flow where the streamwise velocity exceeds the local mean (Lian 1990). Falco (1977, 1983, 1990) found other bursting phenomena called outer layer bursting with the formation of ‘typical eddies’. Falco and Smith, Walker, Haidari, Sobrun (1991) suggested several secondary hairpin vortices. They have each established structural models based on these observations. Several similar structures have been found in a transitional boundary layer. These flows are compared in Table 1.

Table 1 Comparison of the flow structures in transitional and developed turbulent boundary layers

Turbulent Boundary Layer	**Transitional Boundary Layer**
Hairpin vortex (Theodorsen 1952	First closed vortex (Λ-vortex)
Secondary hairpin vortex (Falco 1991, Smith 1991)	Secondary closed vortex
Long streak or streamwise vortex (Kline et al. 1967)	Long streak (CS-soliton)
Typical eddies (Falco 1977, Adrian 2000)	Chain of ring vortices
Streamwise vortex	

The combined visual and quantitative techniques revealed a number of significant features of transitional boundary layers. The physical processes for the formation of the CS-solitons, the Λ-vortex, the secondary closed vortex, the streamwise vortex and the chain of ring vortices are described briefly in this paper. A new model similar to that suggested by Smith et al.(1991), Falco (1991) and Robinson (1990, 1991a,b) is given based on these observations instead of the hairpin vortex.

2. Experimental methods

The experiments were performed in an open-surface recirculating water channel, shown schematically in figure 1. The low-turbulence level water channel in the State Key Laboratory for Turbulence Research and Complex Systems (LTCS) in Peking University had a free stream velocity U_∞ = 20 cm/s with a turbulence level of around 0.1%. The cross-section was 600 mm × 400 mm, and the test section was about 6000 mm long. A flat plate with a chord length of 1.8 m, a span of 0.8 m and a thickness of 15 mm was mounted vertically. Part of the flat plate was above the water surface because the channel top is open. The leading edge had two 90° arcs with different radii. The plate was mounted in the test section at zero angle of attack. The streamwise and spanwise pressure gradients were nearly zero far from the leading edge. A downstream flap was used to make the flow more uniform.

The disturbance generator (T-S wave generator) was a spanwise slit in the plate of length 150 mm and width 1 mm on the working side mounted at a distance x = 200 mm from the leading edge of the plate. Water was periodically pumped in and out of the slit at a frequency of 2 Hz. A water tank was connected to both the slit and two tubes on opposite sides of the plate. A loudspeaker was set on top of a round barrel with the two tubes mounted on the outer edge of the barrel's bottom. The instability waves had a frequency of 2 Hz and an amplitude of 1.8% of the free stream velocity U_0 as set by the voltage input to the loudspeaker. The development of the disturbances in the boundary layer and the structure of the mean flow were investigated with a hot wire anemometer made by Kanomax Company. The hot films were made by TSI. The sensitive part of the probe was less than 2 mm long.

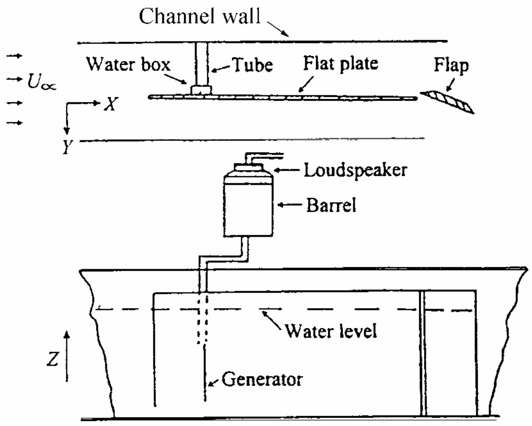

FIGURE 1. Experimental set-up.

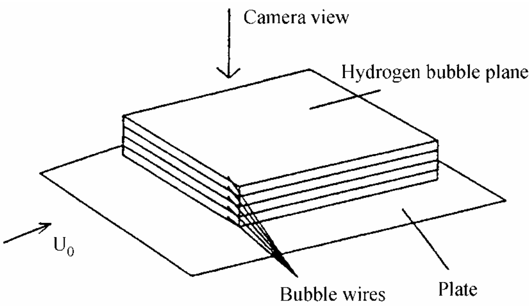

FIGURE 2. Visualization techniques.

Experimental data was acquired from x = 250 mm to 700 mm. At each measured point, three characteristics were measured: the mean value of the streamwise velocity U_0, and the amplitude and phase of the streamwise disturbance velocity, u, filtered at the fundamental frequency. The distributions of these characteristics were measured along the streamwise direction (x), normal to the plate (y) and along the spanwise direction (z).

Along with these measurements, an improved hydrogen bubble technique was used to carefully visualize the flow structures. Complete visualization of the flow structures was accomplished by placing the hydrogen bubble wire at positions from x = 250 mm to 700 mm in steps of 50 mm and from y = 0.25 mm to 6 mm in steps of 0.25 mm. This technique made it possible to clearly visualize the spatial flow structures. As shown in figure 2, different sections in the plan-view were obtained by placing the electrode wire at different y-positions. If the flow was laminar, several hydrogen bubble planes were obtained (figure 2). Continuous plan-views of hydrogen bubbles were produced to visualize the flow structures.

The water temperature during the experiments was about 20^0 C. Constant water temperature was obtained by starting the water channel more than 9 hours before each test. The kinematic viscosity was 1.01×10^{-6} m^2/s and the Reynolds number per meter of length was 2.0×10^5.

Some changes made from our previous experiments (Lee 2000) are as listed in table 2.

Table 2. Changes of operating conditions and flow parameters

	Present	Previous (Lee 2000)
Free stream velocity	20 cm/s	17cm/s
Tollmien-Schlichting wave amplitude	1.8% U_0	1.6%U_0
T-S wave frequency	2 Hz	2 Hz
Formation of the CS-soliton	x = 245 mm	x = 267 mm
Breakdown of ∧-vortex and formation of chain of ring vortices	x = 390 mm	x = 420 mm
Breakdown of the long streak	x = 600 mm	x = 675 mm

3. Experimental results

Figure 3 shows the spanwise distributions of intensity at different y-positions from the surface and at 250 mm, 300 mm, 350 mm and 400 mm downstream from the leading edge. The distributions shown were obtained with a fixed source amplitude. u decreased with the increase of the spanwise distance z from the "peak position" (Bake et al. 2002, Borodulin et al 2002) and became very small for > 10 mm. The spanwise wavelength is about 28mm. We can pay enough attention to the region of z from –14mm to 14 mm

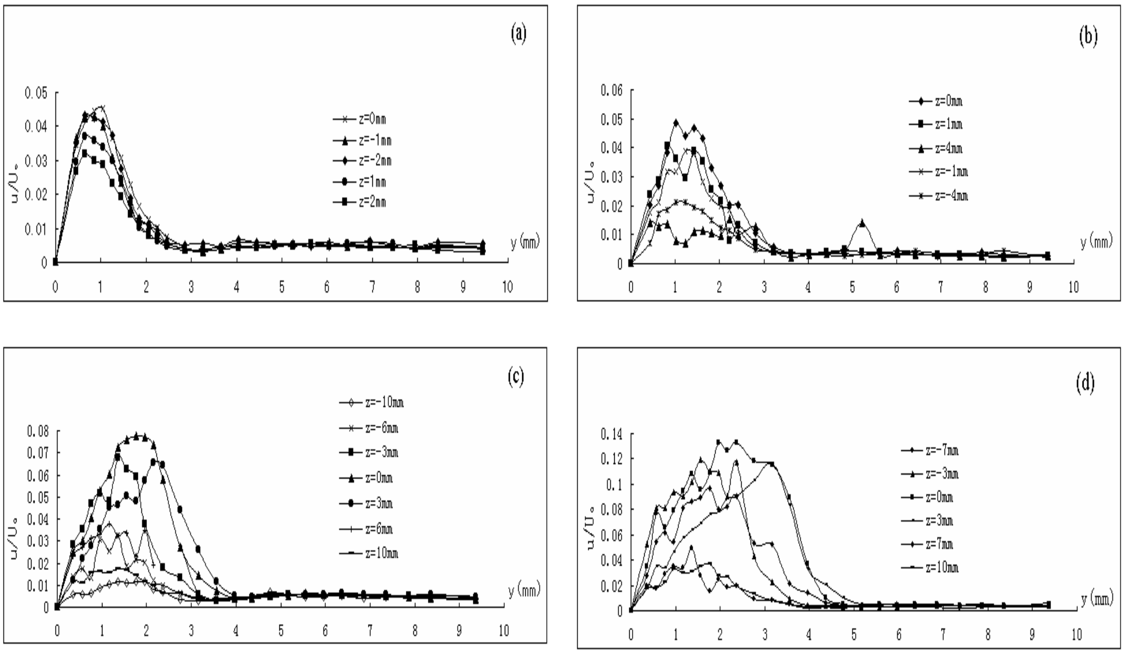

FIGURE 3. Distribution of the intensity of the u-fluctuation across boundary layer: U_∞ = 20 cm/s. (a) x = 250 mm. (b) x = 300 mm. (c) x = 350 mm and (d) x = 400 mm.

Figure 4 show the growth in the wave intensity. The measurements were made along a line corresponding to the "peak position" (z = 0). The intensity is plotted relative to U_∞. The peak and the valley maintained a fixed spanwise position as they intensified in the downstream direction. In contrast to the intensity distribution in the valley, the intensity in the peak increased very rapidly from a minimum value of about 4% at x = 250 mm to a maximum value of about 16% at x = 550 mm. The position of the maximum intensity distributions agrees well with the previous results by Klebanoff (1962).

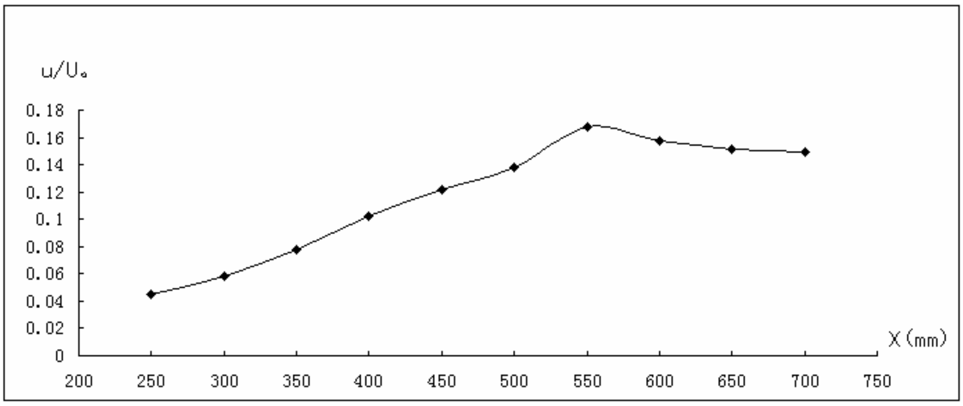

FIGURE 4. Intensity of u-fluctuation at peak for higher wave amplitude.

Figure 5 shows the T-S wave (TS↑) and its evolution using the hydrogen bubble visualization technique. In these pictures, the wire was located parallel to the plate and normal to the direction of the flow and the flow is from the left to right in the pictures. The wire position was moved $\Delta y = 0.25$ mm for each successive picture. The flow is both three-dimensional and unsteady at the peak position (PP↑). The collection of bubbles at the peak position due to fluctuations of both the streamwise velocity components and a spanwise velocity component is the noticeable feature of this region. The streaks waver and oscillate much like a spring carried by a moving train with constant speed. Figure 6 shows the typical T-S wave and its evolution. At the peak position, additional flow structures exist previously called CS-solitons (CSS↑) (Lee 1998, 2000, 2001a,b). Figures 6a and b show a typical Λ-vortex is formed. Two peak positions occurred in this figure. Because these two "peak positions" seemed to be very similar, attention was mainly focused on the upper "peak position". A typical set of oscilloscope traces measured at various distances from the wall is shown in figure 7. The traces show that additional kinks (see arrows) the time traces are periodic and that the phases of the additional kinks (Arrows A) at different y-positions are equal.

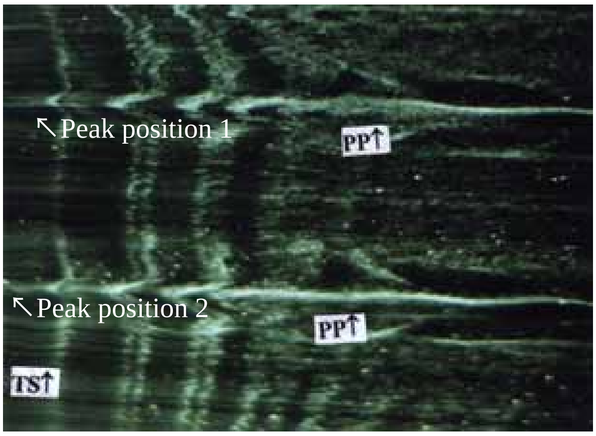

FIGURE 5. Plan-view of the T-S wave (TS↑) and a wavy structure at the two peak positions (PP↑).

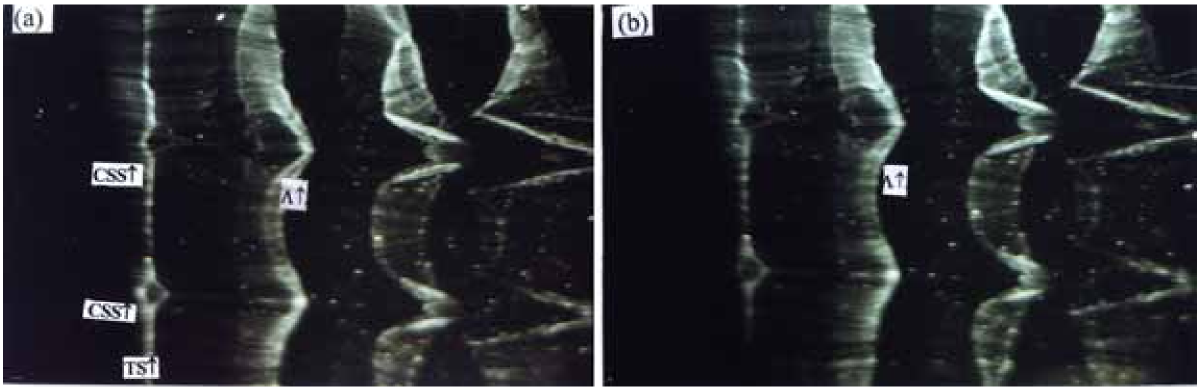

FIGURE 6. T-S wave and its growth. The wire was put at x = 250 mm and y = 0.75 mm.

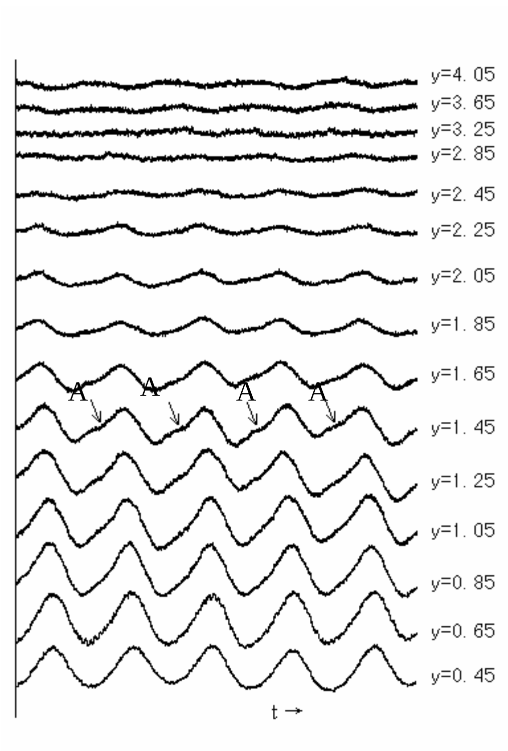

FIGURE 7. Oscilloscope traces of velocity disturbances from the wall at x = 250 mm and z = 1 mm.

4. Formation of the CS-solitons and the Λ-vortex.

4.1. Main features of the CS-solitons

Figures 5 and 6 clearly shown the formation process for the CS-solitons (Lee 1998, 2000) and the so-called Λ-vortex. Figure 5 shows that the CS-solitons formed before the formation of the Λ-vortex. An widely accepted mechanism for the formation of the Λ-vortex was summarized by Hinze (1975) before the detailed visualization such as in figures 5 and 6 and in previous works [31]. A new mechanism has been suggested based on new experimental observations which was described [31]. Figure 8 shows the formation of the CS-solitons and Λ-vortex. The successive pictures show that a kink-like structure appears first which is the initial form of the CS-soliton (CSS↑) and which become a rhombus-like structure finally (B↑).

Figure 9 shows the amplitude variation of the solitons/like coherent structure (Lee 2000) at three y-positions. The measurements were made along a line corresponding to a peak position in the near near-wall region. The low amplitude wave which amplifies and then damps obeys linear theory. At the higher amplitude the wave at the peak first grows as predicted by linear theory, but then exhibits the characteristically different behavior associated with the region of finite amplitude, namely very rapid growth at the peak with initial growth in the valley that is less that of linear theory. Positions A, B, C and D in the figure are different downstream positions at which detailed observations were made, with position A corresponding to the position of the departure from linear theory, position B to the end of the nonlinear interaction and position D to the breakdown of the CS-solitons (Lee 2000). The region from departure to the breakdown of the CS-solitons and the region from breakdown to so-called fully developed turbulent flows which are of principal interest.

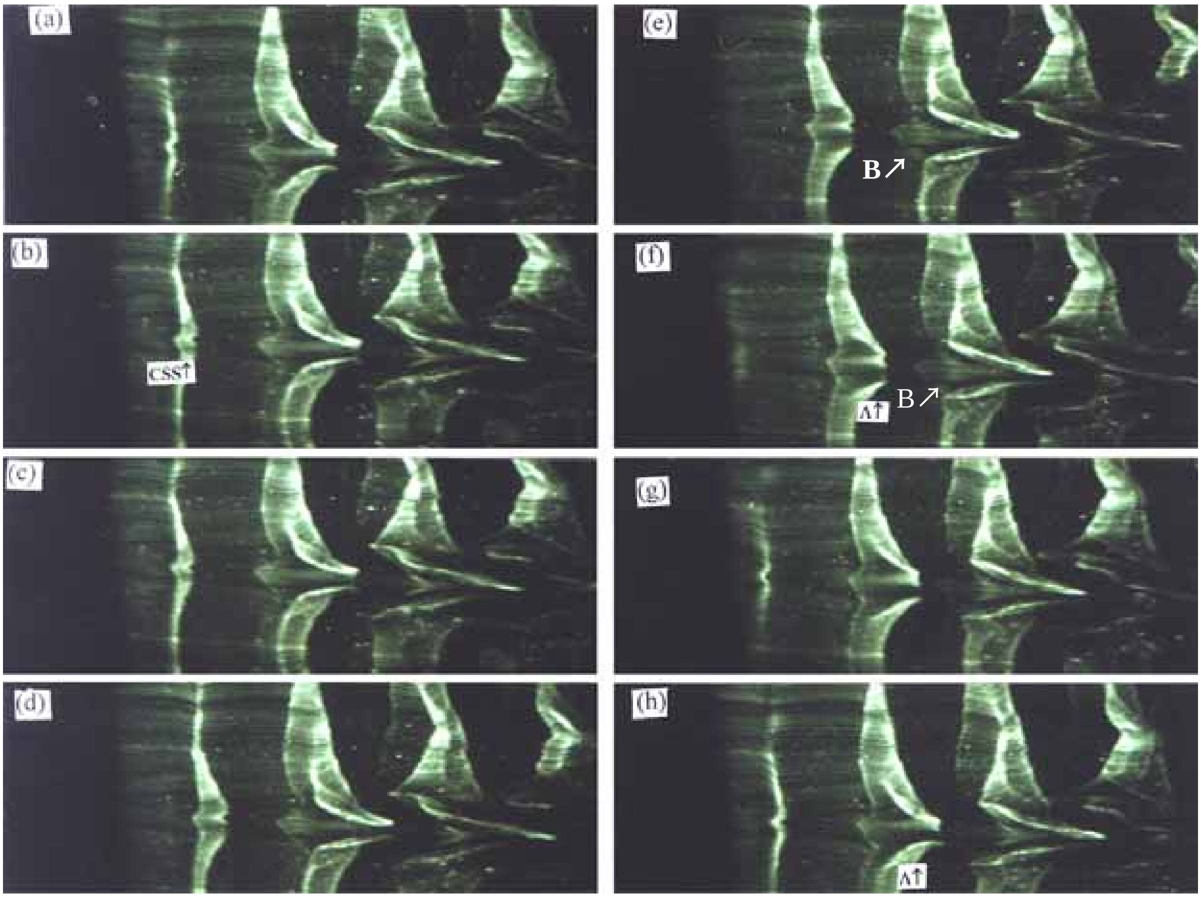

FIGURE 8. Visualization of the formation of the CS-soliton and the well-known Λ-vortex. In these pictures, the wire was located parallel to the plate and normal to the flow direction and the flow was from left to right in the pictures. The wire was positioned at y = 0.75 mm. The time interval between successive pictures was 1/12 s. 1/2 scale from the actual size. Pictures (a) to (f) show the CS-solitons (CSS↑). The formation of the Λ-vortex was was clearly visualized from pictures (e) to (h) (Λ↑).

The measured instantaneous velocity profiles during one period, 0.5 s, are shown in figure 10. With some imagination the occurrence of the CS-solitons and the Λ-vortex in the U-oscillograms can be deduced from the instantaneous velocity profiles. Note that at locations where the U-component has a kink in its distribution, the u-component becomes appreciable. At positions z = –2 mm, the kinks are small. The experimental technique used to draw the time dependent profiles is similar to Kachanov (1994) and Nishioka , Asai & Iida (1989).

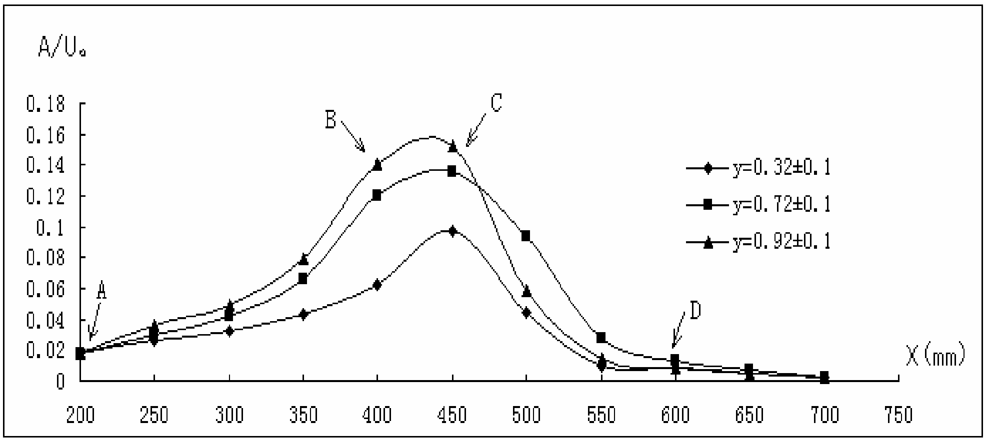

FIGURE 9. Amplitude distributions of the CS-solitons in the x-direction.

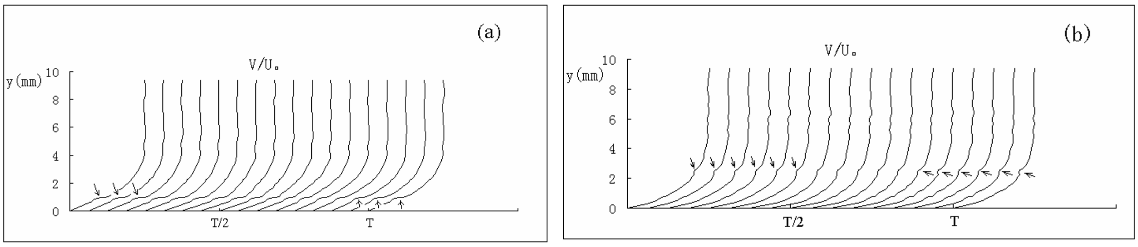

FIGURE10. Low–frequency instantaneous velocity profiles observed at “peak position” (z = 0) and other positions at an early stage (x = 250 mm). (a) z = 0; (b) z = -2 mm.

4.2. Physical mechanism for the CS-soliton formation

Receptivity is defined as the mechanism by which disturbances enter the boundary layer and create the initial conditions for unstable waves. However, only certain kinds of unstable waves can generate the rhombus-like CS-solitons seem in plan-view.

The wave resonant (WR) concept was been suggested (Kachanov 1994) on the basis of a detailed analysis of experiments by Kachanov and Levchenko (1984), as well as of the theoretical results by Craik (1971, 1982). The results obtained by Borodulin and Kachanov (1994) showed that the system of parametric subharmonic resonance, postulated within the framework of the WR concept, was actually observed in the K-regime of breakdown at the stage of spike formation. Simulations of oblique wave interactions in a Blasius boundary layer were performed by Joslin, Street & Chang (1993). Their simulations showed that the oblique wave interaction generates a strong spanwise-dependent mean-flow distortion. No two-dimensional (2D) T-S waves take part in this process but the CS-solitons can generate this kind of strong spanwise-dependent mean-flow distortion. Williamson and Williamson and Prasad [51] found a honeycomb pattern which is considered to be the direct result of an interaction between oblique shedding vortices and two-dimensional large-scale waves that grow in the far wake. One possible physical reason for it is that the CS-solitons are generated by the interaction between two oblique waves. The effect of two-dimensional T-S waves ont the formation of the CS-solitons was investigated using theoretical approach called Phase-locked which showed that the two-dimensional T-S wave has a catalytic effect on the three-dimensional structure formation. Very recently, a self-consistent asymptotic theory developed by Wu et al.(2001) showed that the instability of the perturbed flow is governed by a remarkable simple system, a Schrödinger equation. The instability modes can be viewed as a kind of modified oblique T-S wave. Because of these modified T-S wave are governed by the Schrödinger equation. The solution seems to be a kind of solitons like structure. In fact, the oblique waves may exist anywhere because they are induced by any three-dimensional disturbance. Figure 11 displays the oscilloscope traces of the velocity disturbances at various distances from the wall for different z at the same x (x = 300 mm). An additional flow structure was generated periodically as clearly shown in figures

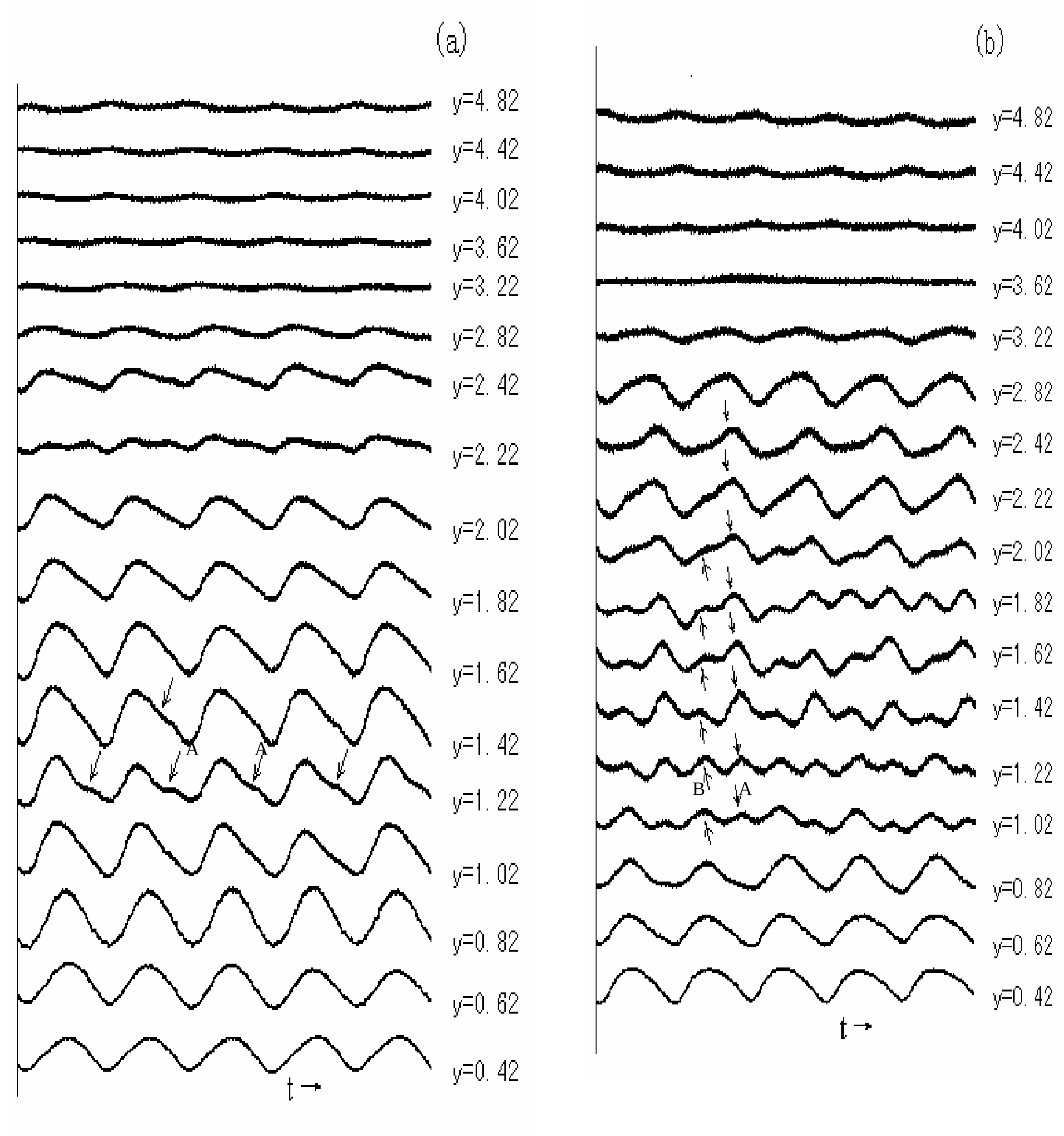

FIGURE 11. Oscilloscope traces of velocity disturbances at various distances from the wall. (a) x = 300 mm, z = 1 mm; (b) x = 300 mm, z = 4 mm.

11a and b. Note the velocity fluctuations at y = 1.22 mm and 1.42 mm. The CS-soliton evolving from a basic wave was measured at x = 250 mm, with the new structure which lags behind the basic wave , figure 7. The same new structure was most apparent at x = 300 mm, z = 4 mm, from y = 1.02 mm to y = 2.22 mm. The structure was created in the valleys of the CS-solitons in the near-wall region, with the amplitudes of the additional kinks varying from a minimum at y = 1.02 mm to a maximum at y = 2.82 mm, while the basic wave varies from a maximum at y = 1.02 mm to a minimum at y = 2.82 mm. This detail has never been observed before. At x = 300 mm, the visualization results in figures 6 and 8 show that two kinds of flow structures, CS-solitons (arrows B) and Λ-vortices, exist. The additional kinks (see arrows A) were generated by the Λ-vortices.

Some scientists believe that the CS-solitons are secondary flow structures generated by the

Λ-structures. However, the curves in figure 9 provide no evidence that the Λ-structures were formed before the CS-soliton. Actually, motion video clearly showed that the CS-solitons formed slightly before, as suggested by Lee (2000, 2001a,b).

The occurrence of a pocket vortex in a turbulent boundary layer has been suggested by Falco (1977, 1991) and Smith et al. (1991). A pocket can form as the result of the interaction of a passing typical eddy with the wall and the sublayer, as a result of the lift-up and formation of the hairpin vortices , and by the induction of outer fluid towards the wall by strong streamwise vortices. Moin, Leonard and Kim (1986) have shown that a sufficient concentration of markers covering an area on the wall is needed to detect pocket vortex, and that hydrogen bubble visualization does not provide enough marker, in general, to observe them. The pocket vortex becomes highly stretched because it induces itself to remain within the boundary layer. Furthermore, because it is so close to the wall the impermeability condition is important which adds to the stretching. Markers will buildup on the outer sides of the pocket vortex, where fluid is moving away from the wall forming a pair of streaks along the sides of the pocket . The mechanism for this lift-up of markers appears to be well described by Doligalski and Walker (1984). The elongation of the pocket vortex, from the moment of its formation, continually reforms the upstream and lateral boundaries of the pocket. This was clearly observed in the high-speed movies of Falco (1991). Smith et al. (1991) also noted that the upstream kinks of bent vortex tubes would have the 'most active' viscous response. A further consequence of this stretching is that the pocket vortex is rapidly dissipated leaving behind a pair of streaks inside the long streak pair.

4.3. CS-solitons and turbulent spots

A turbulent spot was first found by Emmons (1951). A nice picture of a growing turbulent spot in plan view was obtained by Elder (1960). Note that the flow condition upstream of the turbulent spot, after the spot passes, is again laminar. Earlier, other investigators observed the existence of turbulence spots during the transition process (Schubauer et al. 1956, Mitchner 1954). Landahl (1977) analyzed the effects of initial "lift-ups" i.e. localized three-dimensional up-down movements in the high $\partial u/\partial y$ regions of a laminar boundary layer. Inviscid linear theory indicates algebraic growth due to the straining action. If in real flows, the growing disturbance exceeds a nonlinear threshold before its viscous decay, it could open up a relatively low level bypass to a small turbulent spot. Numerical inviscid evolution in a Blasius layer, experiments on weak (non-bypass) and stronger (bypass) "lift-ups", and Navier-Stokes simulations of the latter, disclose (besides the Gaster-Grant 1975 Laminar T-S spots) rather similar patterns of intensifying shear over the center of the disturbance and elongating flow structures on the sides. For stronger disturbances, the breakdown seems to be associated with long strips of high-speed fluid surrounding a low-speed region and with rapid inflectional instability of the distorted mean profile.

Kachanov (1994) suggested a new transition called "without turbulent spot transition". They believed that the only condition that must be satisfied to generate turbulent spots is that the initial instability wave must have sufficiently strong temporal modulation in its initial amplitude. The so-called microscopic have also been suggested for the onset of turbulent spots (1994).

Lee (1998, 2000, 2001a,b) discussed the differences between CS-solitons the turbulent spots. The main conclusions are described in table 3.

Table 3. Differences between a CS-soliton and a **real** turbulent spot

	CS-soliton	***Turbulent spot***
Location	appears at early stage	appears at further downstream
Structure	simple wave-like	Several CS-solitons and their bounded vortices
Scales	single scale	Multi-scales

Previous studies must be carefully analyzed to distinguish between a real CS-soliton and a turbulent spot. As described by Theodorsen (1952), turbulent bursts may be identified with turbulent spots, i.e., the appearance of turbulent spots is associated with localized turbulence. Lee (2000) also suggested the differences between CS-solitons and turbulent spots.

5. Secondary closed vortex

Figure 12 shows a new closed structure (SCV↑) separated from the CS-solitons (Arrows B) that has never been reported in transitional boundary layers. Falco (1991) and Smith et al. (1991) observed the so-called secondary closed hairpin vortex in a turbulent boundary layer with adverse pressure gradient. As sketched by Smith (1991), a new mechanism called surface layer separation can be provoked by a symmetric hairpin vortex at three locations, namely behind the head and immediately inboard of each leg.

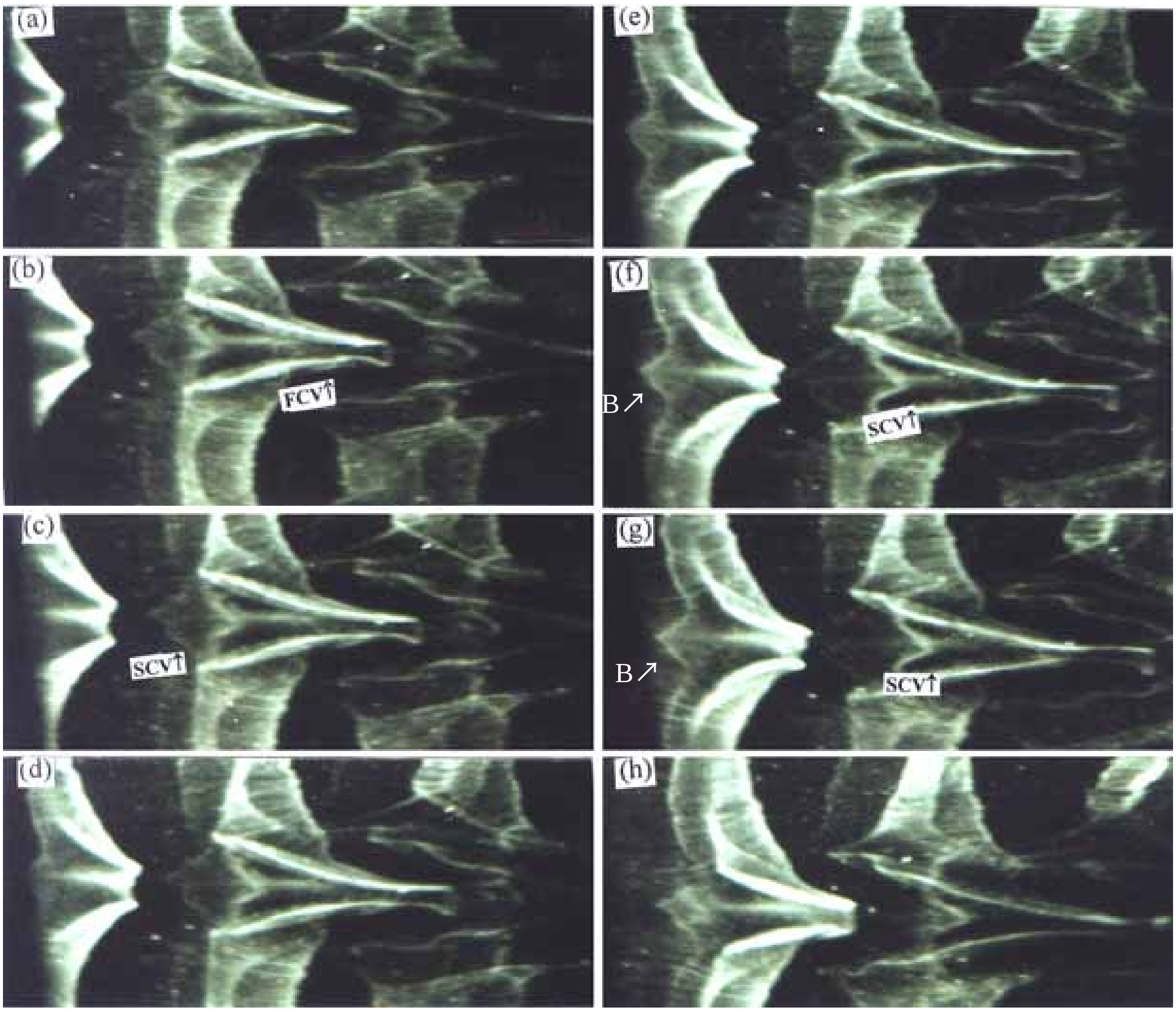

FIGURE12 Secondary closed-vortex (SCV↑) formation. (a)-(d) Part of the first closed vortex, i.e., the Λ-vortex and a CS-soliton appear (CSS↑). (e)-(h) The right-hand side of the secondary closed vortex appears and is then separated from the CS-soliton. At the same time, the Λ-vortex is stretched (FCV↑). The time interval between successive pictures is 1/12 s. The figure is 1/2 of actual size and the flow is from left to right. The hydrogen bubble wire was located parallel to the plate and normal to the flow direction. The wire position was x = 300 mm from the leading edge and y = 1.25 mm from the wall.

Figure 13 shows the flow structures from the near wall region to the outer layer. The secondary closed vortex (SV↑) has not been reported in a transitional boundary layer before. The wire was moved Δy = 0.25 mm for each step shown in the picture series. Figure 13(a) shows a long streak (L↑) and its evolution at different times. The rotation of this long streak has not been observed indicating that the long streak behavior differs from that of the streamwise vortices. However, two streamwise vortices exist on the two sides of the long streak. The long streak (L↑) is also present in figure 13 (b). The structure is modulated in time with the fundamental frequency. The long streak in a transitional boundary layer is different from that in a developed turbulent boundary layer in several aspects. First, the long streaks in a transitional boundary layer appear in the near-wall region in the "peak positions". But the long streaks called streamwise vortices in a developed turbulent boundary layer appear both at the interface between the high-speed streaks and the low-speed streaks and in the near-wall region. Secondly, the long streaks in a transitional boundary layer represent the features of the CS-solitons (CSS↑). A complete long streak is composed of several CS-solitons as clearly shown in figure 13 (b). In figure 13 (c), the two middle parts of the Λ-vortex on the two sides of the long streak rotate at a much higher speed. Therefore, two horn-like vortex tubes (VT↑ and VT↓) are formed on the two sides of the long streak, which causes interaction between the secondary closed vortex and the Λ-vortex. The left-hand side of the secondary closed vortex can be seen in figure13(c) (SV↑). The two vortex tubes formed on the two sides of the "peak position" in figure 13 (c). They then develop downstream and become very strong. The left part of the secondary closed vortex is also present (see the “peak position” in all the figures). It is separated from a CS-soliton [1998, 31]. A long streak and two vortex tubes are seen in figure 13(d). The tubes look similar to a sheep's horn. One or two vortices in a chain of ring vortices (C↑) also appear. The interaction between the long streak and the chain of ring vortices is also shown here. A perfect secondary closed vortex is shown in figures 13(e) and (f) (SV↑) which is completely closed instead of in the Λ-like form. Figure 13 (f) shows the formation of the secondary closed vortex (SV↑). Figure 13(g) shows both the streamwise vortices (SW↑) and the left part of the secondary closed vortex (Arrow A). The existence of this left part of the vortex shows the secondary closed vortex is different from the form of the Λ-vortex. The pictures illustrate the interaction between the secondary closed vortex and the side-part of the Λ-vortex. Besides the two vortex tubes, the filaments from both the Λ-vortex and the secondary closed vortex are twisted together.

The pictures in figures 12 and 13 show several new features. (a). The secondary vortex is closed instead of a hairpin vortex. (b) The additional hairpin vortices on the two legs of the main hairpin vortex were not found. (c) The development of the instability along the borders of the CS-solitons is the necessary condition for the separation of the secondary closed vortex from the CS-solitons (Lee 1998). (d) We do not argue that the original work by Smith et al. was in error, but merely incomplete.

A different mechanism is suggested for the different vortex form which is similar to an earlier proposal by Lee (2000, 2001a,b) had been suggested. The quantitative results are present but do not clearly show which kinks were generated by which structures (figure 14). At this stage, there exist four kinds of flow structures which have strong effects on the time traces, the CS-solitons, the Λ-vortices, the secondary closed vortices and the first ring vortices which will be discussed lately. After extensive with the figures, the kinks indicated by arrows A, B, C and D were related to the CS-solitons, the Λ-vortices, the first ring vortices and the secondary closed vortices , respectively.

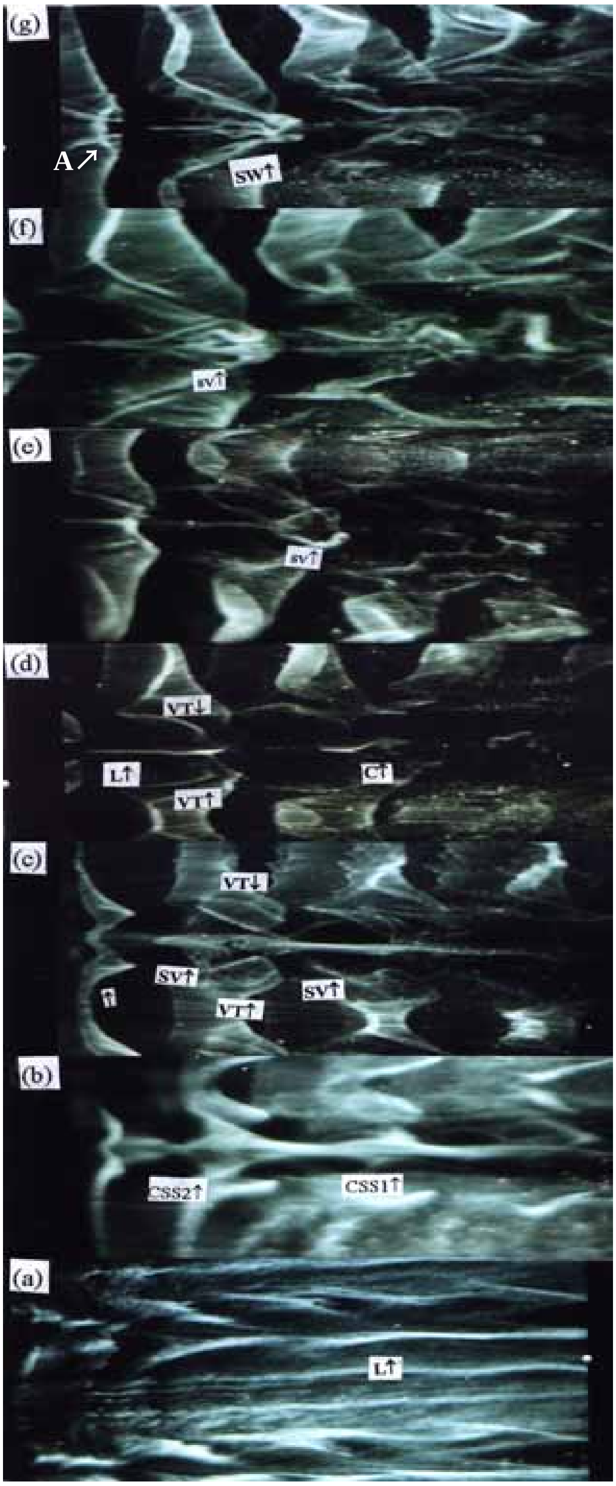

FIGURE13. Flow structures at different y-positions. The hydrogen bubble wires were located at x = 350 mm and y = 0.25 mm, 0.5 mm; 0.75 mm; 1.0 mm; 1.25 mm; 1.5 mm and 1.75 mm for the 7 photos. 9/10 scale from the actual size of the photos

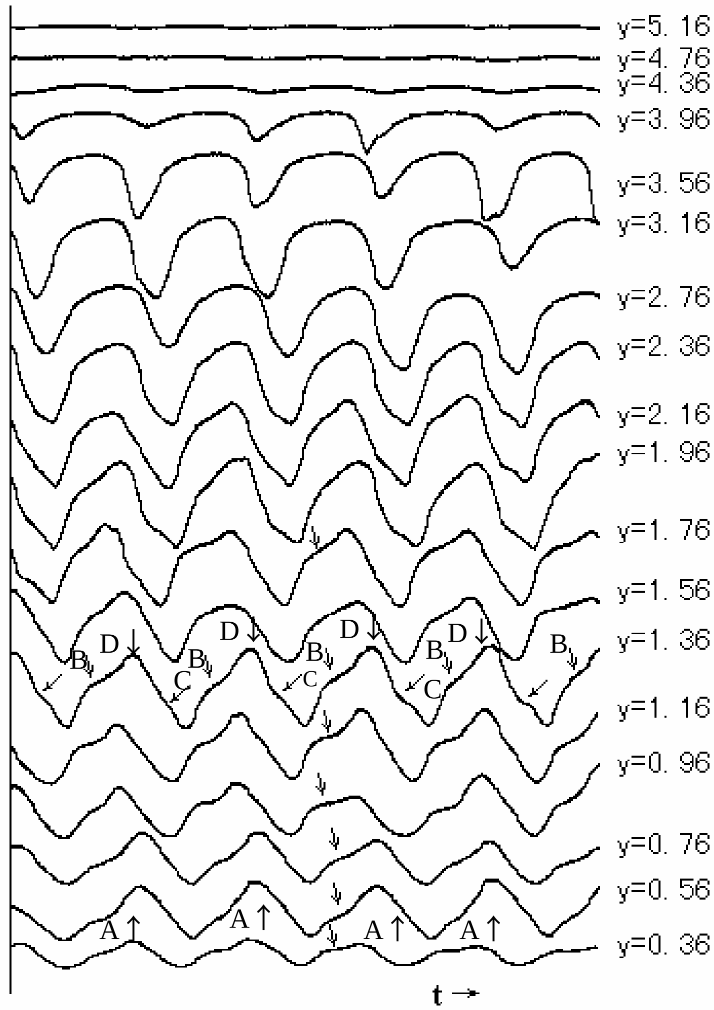

FIGURE14. Oscilloscope traces of the velocity disturbances at various distances from the wall at x = 400 mm for z = 0.

6. Formation of the chain of ring vortices

The typical eddies was first noticed by Falco (1977, 1990). As described by Falco, the typical eddies are local compact regions of vorticity concentration that have distorted vortex ring configurations and behavior. The measured frequency of occurrence of the typical eddies, when normalized by the free stream velocity and boundary layer thickness, $f\delta/U_\infty$, increase from 0.78 to 1.16 as Re_θ increases from 753 to 3853. Falco's overall sense obtained from several thousand feet of visual data taken with high-speed cameras, as well as time observations of lower speed boundary layers, and the cross-light sheet experiments of Falco described, is that the typical eddies have a vortex ring configuration and evolution, as opposed to an attached hairpin eddy configuration and evolution. At low and moderate Reynolds numbers the typical eddies appear to be laminar vortex rings, and thus are viscous controlled. At higher Reynolds numbers, the typical eddies have been observed to appear as wavy cored vortex rings. At still higher Reynolds numbers (such as characteristic of atmospheric boundary layers), they have been observed, as completely typical eddy motions. The formation and evolution of typical eddies in a highly perturbed vortex environment strongly governs the shape of these eddies. It is unrealistic to expect that an observer will often see an idealized picture of a developing or developed typical eddy. Therefore, understanding of the formation process is not yet complete, but there are indications that at least two mechanisms are involved. Formation could take place by pinch-off and reconnection of hairpins observed to lift-up from the wall (see, for example, Melander & Zabuski 1988). Falco (1977,199) presented data showing evolution by this process. The experiments of Chu & Falco [42] show the reconnection of hairpin vortices, as do the numerical simulations of Moin et al.(1986). The other likely mechanism is the formation of typical eddies from an instability of a local region of highly vortical fluid to an applied force, as described by the solutions of Cantwell (1986). These solutions describe the formation of the vortex rings in an infinite fluid through the action of an impulsive force on a vortical region.

As with Falco, Borodulin et al.(2002) and Bake et al. (2002) suggested a simple formation process for the high frequency vortex ring formation in a transitional boundary layer called self-induction of the two legs of the Λ-vortex.

Lee (2000, 2001a,b) used experimental observations to suggest a new process which describes how continuous separations along the border of the CS-solitons can generate high frequency vortices.

The chain of ring vortices (CRV) shown in figure 15 were shown to be as periodic instead of random as described in our previous works as well as in recent works (see, for examples, Lee 2000, 2001a,b and Borodulin et al. 2002).

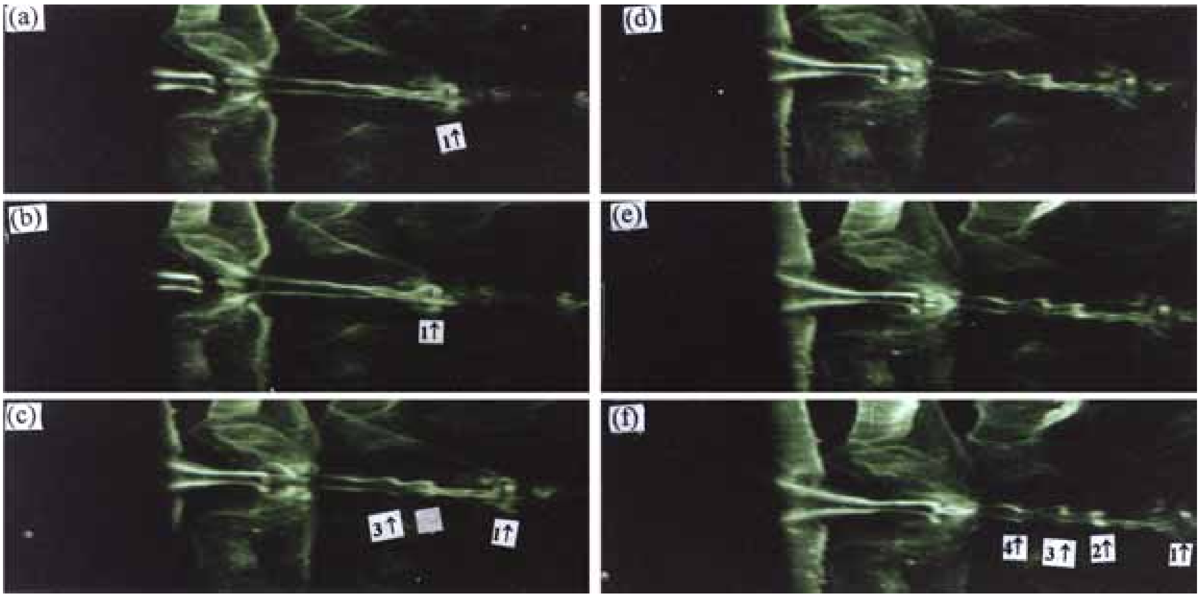

FIGURE 15. Plan-view of the chain of ring vortices (↑) associated with a Λ-vortex (A↑) (the wire was at x = 360 mm and y = 1.75 mm) (See Lee 2001). 1/2 scale from the actual sizes of all photos). The first ring vortex propagated downstream (1↑) while the other three (2↑, 3↑ and 4↑) appeared at nearly the same time. The time interval between successive pictures was 1/24 s. Figure 15 (a) shows the first ring vortex. Figures 15(b) to (e) show the other three ring vortices.

A secondary closed vortex appeared after the formation of the Λ-vortex (figures14, 15 and 16). Lee earlier suggested the possibility of the existence of this kind of closed vortex just based on the visual observation by Lee (2001a) . The direction of the rotation velocity in this vortex is the same as in a Λ-vortex. The angle between the plane with the closed vortex and the flat plate is less than that between the plane with the Λ-vortex and the flat plate but the y-position of the closed vortex is higher than that of the Λ-vortex at the same x-position. Since the closed vortex has a higher downstream convection velocity compared with the Λ-vortex, they will eventually meet each other. Figure 16 shows the different stages of this secondary closed vortex interacting with the two legs of the Λ-vortex. Figure 16(a) shows the closed vortex close to the two legs of the Λ-vortex as it catches up to Λ-vortex. Figure 16(b) shows that when the two vortices are close to one another, the interaction causes the rotational velocities of both vortices to increase. The Λ-vortex is divided into three sections: the head part, the interaction part and the upstream part. The filaments connecting the head part where an Ω-shaped vortex has formed and the left part of the Λ-vortex become much more slender and will break when their rotational velocity is sufficiently large, figures 16(c) to (d). The Ω-shaped vortex was found many years ago (Hama et al. 1963, Knapp et al 1968) but was more recently found to be the first ring vortex in the chain of ring vortices (Lee 2000, Borodulin et al. 2002, Bake et al. 2002). Few studies after the works by Crow (1970) and Moin et al.(1986)

have analyzed the physical mechanism for the formation of the Ω-shaped vortex because researchers such as Bake et al. (2002) believed that it is induced by vortex stretching and self-induction.

In general, The first ring vortex forms due to vortex stretching, induction by the secondary closed vortex, and axial instability of the vortex filaments. Vortex stretching is well-known effect so it is not repeated here. The induction of the secondary closed vortex which bring the two legs of the Λ-vortex close to each other is shown in figure 16. This effect, which is needed to describe the axial instability of the vortex filament, has not been previously suggested in boundary layer flow.

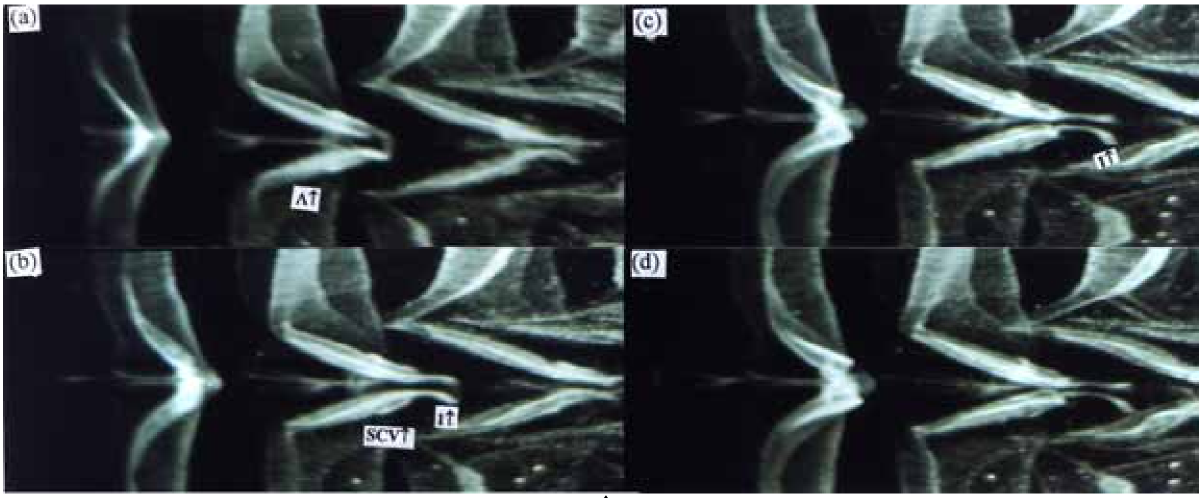

FIGURE 16. Generation of the first ring vortex (1↑) by the interaction between the secondary closed vortex (SCV↑) and the Λ-vortex (Λ↑) (Lee 2001a). The hydrogen bubble wire is at x = 250 mm and y = 1 mm from the leading edge of the flat plate and the time interval between successive pictures is 1/12 s. 9/10 scale from the actual sizes of the photos.

Several later stages of the interaction between the Λ-vortex and the secondary closed vortex are clearly seen in figures 17(a)-(l). Two symmetric filaments appearing on the inside-face of the Λ-vortex in the interaction zone are observed to move into the center of the secondary closed vortex. The middle parts of the two filaments look like two half-ring vortices appearing symmetrically in the center of the secondary closed vortex. At the same time, the parts of the two filaments in the head part move from the inside out due to the secondary closed vortex because of a positive angle between the Λ-vortex and the flat plate. For the same reason, the filaments in the upstream parts then go into the secondary closed vortex so that two narrow necks of these two symmetric filaments exist inside the secondary closed vortex. After the two symmetric filaments meet each other where their two narrow necks come together, they break and reconnect into three small ring vortices. The filaments of the third ring vortex come from the two symmetric filaments. The second and fourth ring vortices are the direct results of the breaking and reconnecting of the filaments of the Λ-vortex and the secondary closed vortex. The filaments on the right hand side of the fourth vortex come from the Λ-vortex while those on the left-hand side come from the secondary closed vortex, The filaments on the left-hand side of the second vortex come from the Λ-vortex while those on the right hand side from the secondary closed vortex. The second, third and fourth ring vortices then move from the inside to the outside of the secondary closed vortex, are lifted up to higher y-positions and then propagate downstream at a higher convection velocity relative to the Λ-vortex because a positive induction velocity field exists in the y-direction at the center of the secondary closed vortex.

When two vortex filaments are brought into contact by an induced velocity field, viscous diffusion in the contact region causes annihilation of vorticity. The annihilation of vorticity effectively “severs” the filaments and, due to the kinematic constraint that vortex lines can not end inside a field, they reconnect on either side of the contact region. Various different views on vortex breaking and reconnection were given by Saffman(1972,1990), Zawadzki & Aref (1991), Melander &. Hussain(1989), Kokshaysky1979), Rott (1956), Sears (1956).

,

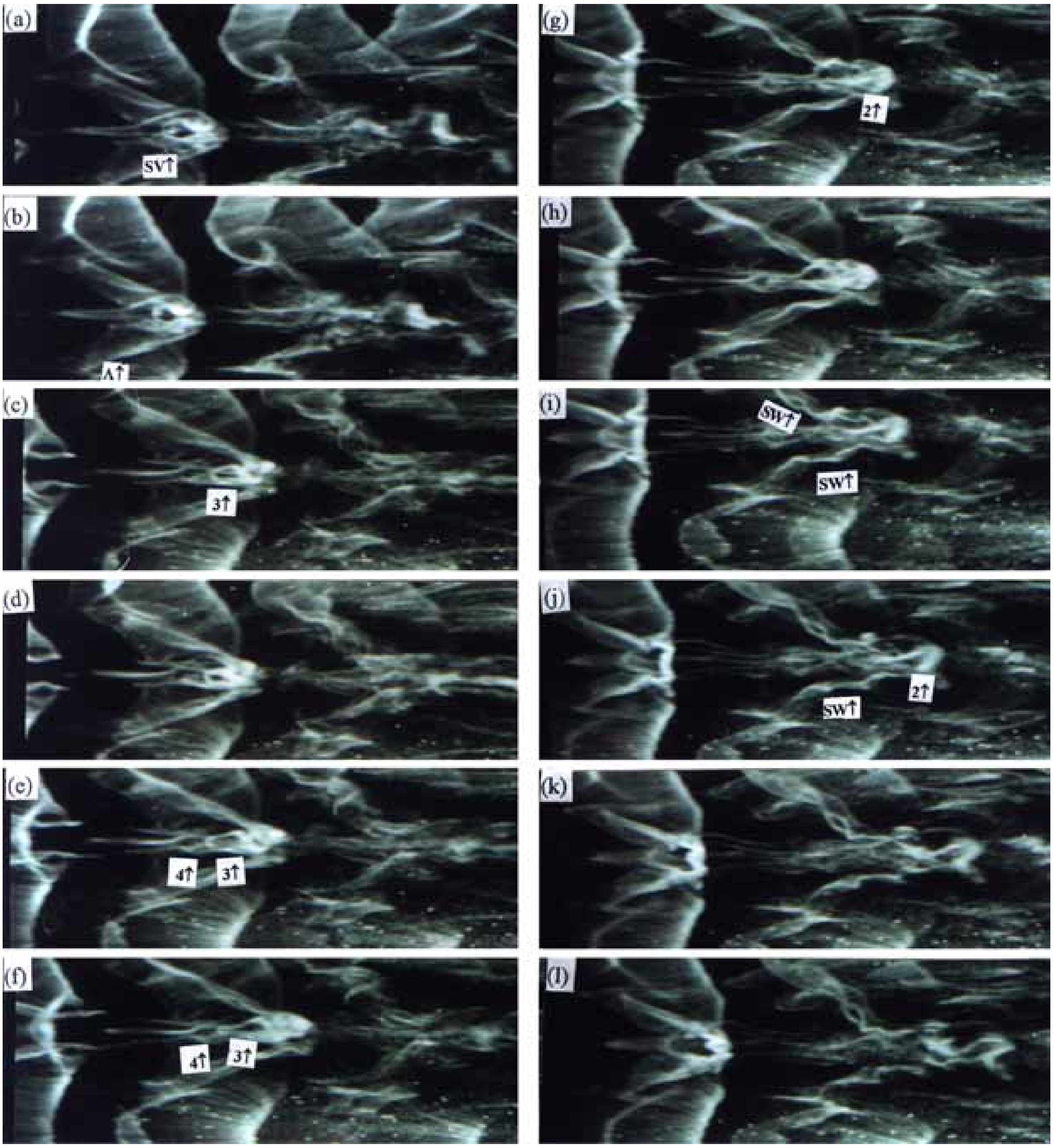

FIGURE 17. Formation of the second (2↑), third (3↑) and fourth (4↑) ring vortices in a chain of ring vortices by Lee (2001a). The hydrogen bubble wire was at x = 350 mm and y = 1.5 mm. The time interval between successive pictures was 1/24 s. 1/2 scale from the actual sizes of the photos. Figure 17(a) shows the filaments of the Λ-vortex moving into the center of the secondary closed vortex (SCV↑) and the two symmetric filaments with two narrow necks formed inside the center of the secondary closed vortex. Figure 17(c) shows the breaking and reconnection of the two symmetric filaments at their narrow necks inside the secondary closed vortex and the third ring vortex is clearly seen. In figures 17(e) to (f), the fourth ring vortex appears. The filament on the left-hand side of the vortex comes from the secondary closed vortex and the filament on the right-hand side of the vortex from the symmetric ones. Figures 17(h) to (k) show the formation of the second ring vortex. The filaments of this vortex come from both the secondary closed vortex and the two symmetric filaments. All three ring vortices appear clearly in Figures 17(i)-(k). Two stream-wise vortices appear (SW↑) on the two sides of these three vortices, which are the well-known stream-wise vortices also known as long streaks. The filaments of the stream-wise vortex come from both the secondary closed vortex and the Λ-vortex.

Figure 18 shows the measurement data which is generated by the chain of ring vortices. The number of the spikes in a period equals that of the vortices in a chain.

Both the measured data and the visual results show that the existence of the interaction between the Λ-vortex and the secondary closed vortices. Different from Borodulin et al.(2002), Bake et al. (2002), a new mechanism for the formation of the chain of ring vortices is suggested based on the previous visual study (figures 15, 16 and 17) and the present quantitative and visual results (figures 14, 15 and 18) ‘

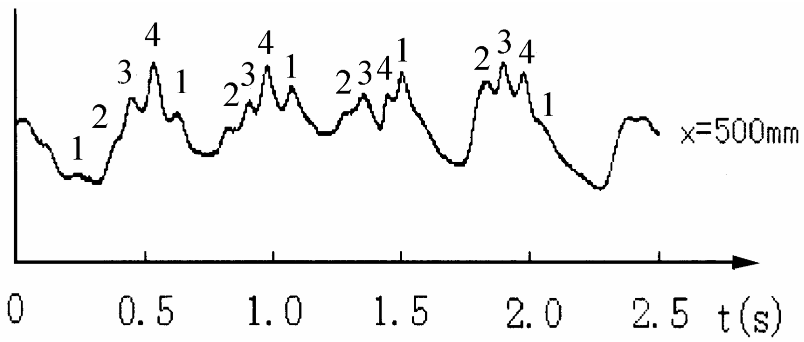

FIGURE 18. Oscilloscope traces of the velocity disturbances at x = 500 mm, y= 1.5 mm, z = 0.

7. Breakdown of the chain of ring vortices

The regular breakdown of the chain of ring vortices is shown in boundary layer transition in figure 20. At first the filaments of the ring vortex are twisted back and forth in a regular pattern. Then the filaments are broken on the near wall side (arrows) and finally broken completely. The breakdown of the other three ring vortices in the chain occurs in a similar manner as with the first ring vortex, as seen on a video of the whole process. Typical velocity fluctuations and frequency spectrums of the chain of ring vortices and after its breakdown are illustrated in figure 19. At the breakdown stage of the chain of ring vortices, the vortices produce a wide spectrum of strongly coupled frequencies. The videos showed that the breakdown was nearly periodic. Observation of the process showed solid bridge connecting the high frequency vortex (4-spike stages) to the much higher frequency velocity fluctuations in figure 20.

Direct comparison of the measured and visualized results presented here demonstrates that the breakdown of the chain of ring vortices plays an important role in the late stages of transition. They excite the near wall region around the peak position producing very intense vortex fluctuations in the boundary layer. But obvious contributions to the flow randomization process by the breakdown have not been found. The properties of the frequency spectrum during the chain of ring vortices and after their breakdown, figures 19 and 20, describe the deterministic features of the breakdown near the last stage of transition which have not been previously reported. These results will facilitate understanding of the later stage of transition.

8. Formation of the streamwise vortices

A streamwise vortex is a typical coherent structure in both transitional and developed turbulent boundary layers. Streamwise vortices were observed early in the history of turbulent structure research.

4↑).

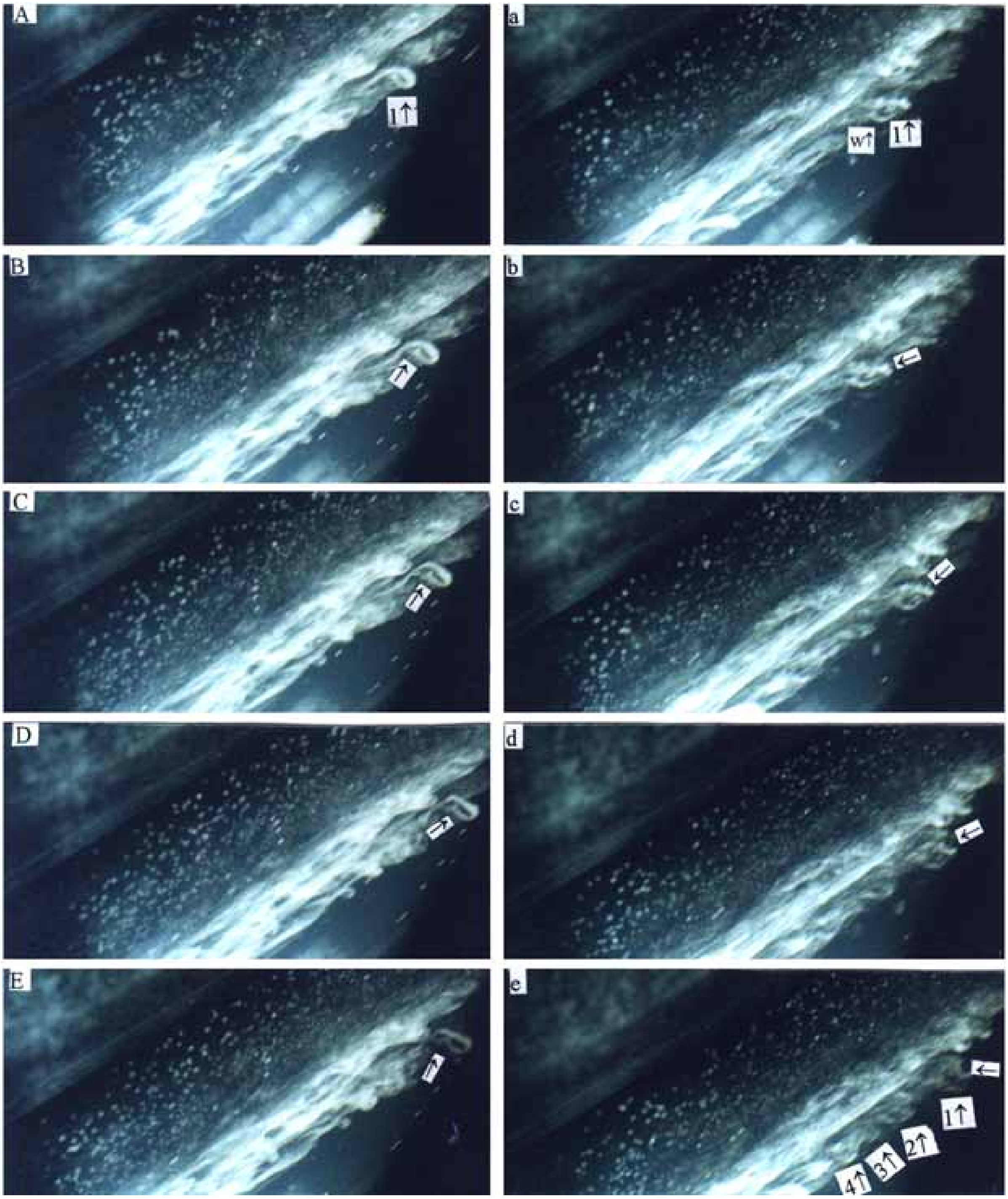

FIGURE 19. Breakdown of the first ring vortex in a transitional boundary layer. A-E, Breakdown of the near wall part of the vortex. In A, the first ring vortex appear. Arrows point out the position of the breakdown in the near wall region of the boundary layer. a-e, Breakdown of the first ring vortex in the outer region of the boundary layer. a, The vortex in the outer layer starts to break (1↑) and the vortex in the near wall region had already broken (W↑). In c, d, and e, arrows show the points of the breakdown. In photo e, the state of the first ring vortex and with other ring vortices in a chain appears (1↑, 2↑, 3↑ and 4↑).

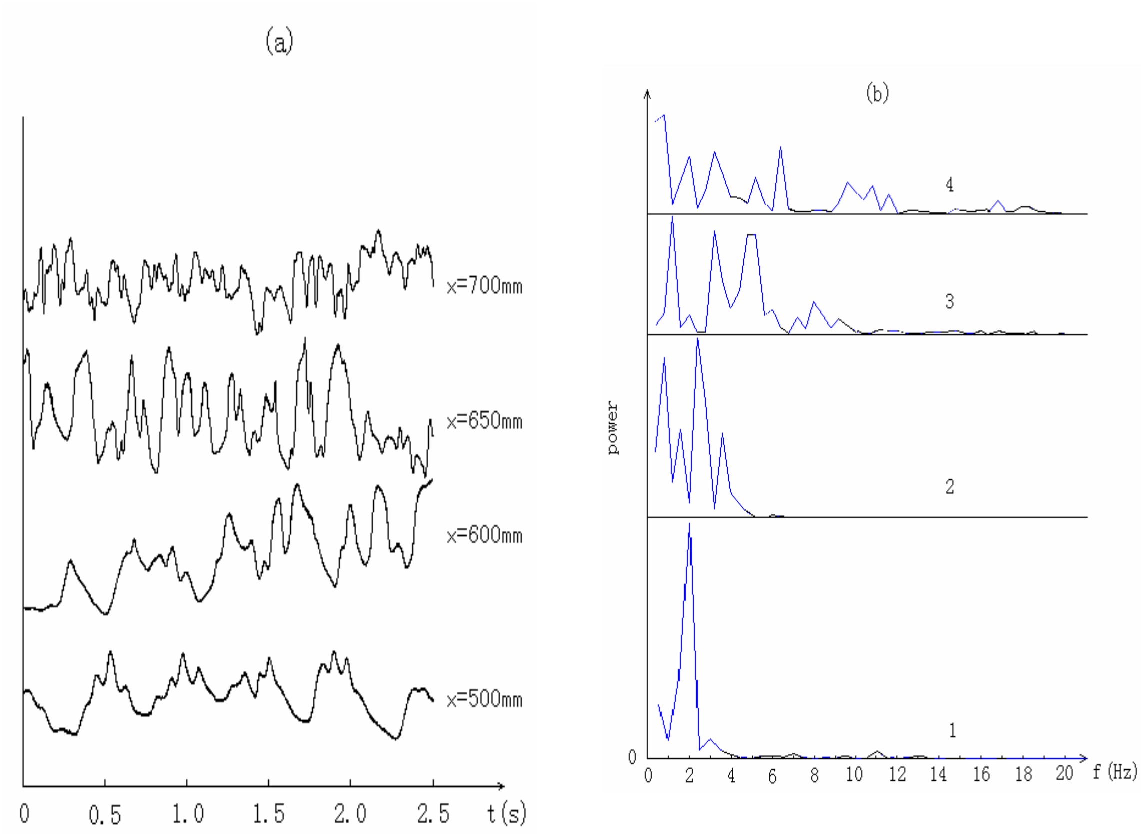

FIGURE 20. Time traces starting from the 4-spike stage to the multiple spike stage and their corresponding spectra. The Tollmien-Schlichting wave frequency was 2 Hz. Lines 1, 2, 3, and 4 on the right side of the figure are the spectra at x = 500 mm, 600 mm, 650 mm and 700 mm.

Kline et al. (1967) and Kim, Kline & Renolds (1970) noted the common appearance of quasi-streamwise vortices in conjunction with the oscillation phase in the turbulence-generating bursting process. Clark and Markland (1971) made careful observations of relatively long quasi-streamwise vortices with 3 to 7 degrees upward tilt in the wall region of a turbulent water channel.

Perhaps the most extensive direct information concerning quasi-streamwise vortices came from the end-view hydrogen bubble visualization studies of Smith et al. (1991). These studies confirmed the common occurrence of quasi-streamwise vortices in the near-wall region, including frequent observation of counter-rotating pairs. In the simultaneous top and end views by Smith and Schwartz (1983), counter-rotating pairs in the near wall region were always associated in space and time with low-speed streak formation. The study by Kasagi (1988) suggest that quasi-streamwise vortices are more common than vortex pairs in the near-wall region, and that the vortical structures are not as long as the near-wall low-speed streaks.

Lee (2000, 2001a,b) analyzed almost all of the structures referred to as streamwise vortices and found that there are two different kinds of flow structures which have been referred to as streamwise vortices. One is the real streamwise vortex such as that found by Clack & Markland (1971) and Lian (1990). The other is the long streak containing several CS-solitons, which is called a solitary quasi-streamwise vortex by Kasagi (1988). For example, the long streak very near the wall found by Kline et al.(1967) was actually a solitary quasi-streamwise streak instead of a streamwise vortex.

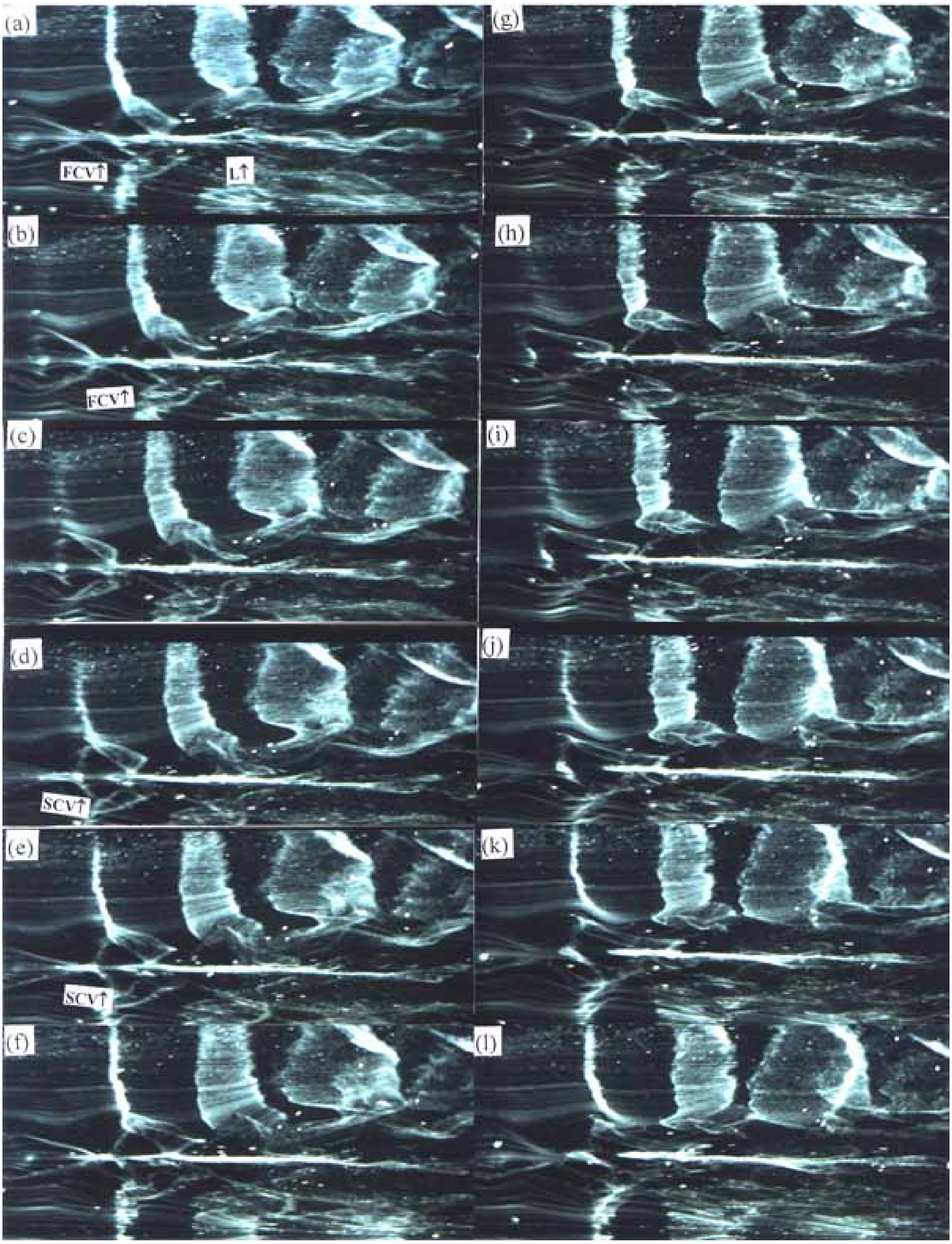

FIGURE 21 Flow structures at x = 400 mm. The wire was at y = 0.75 mm. (b) and (c) The left-hand side of the first closed vortex appears (FCV↑). The complete secondary closed vortex appears in (d), (e) and (f) (SCV↑). A long streak associated with two streamwise vortices is always present in the "peak position".

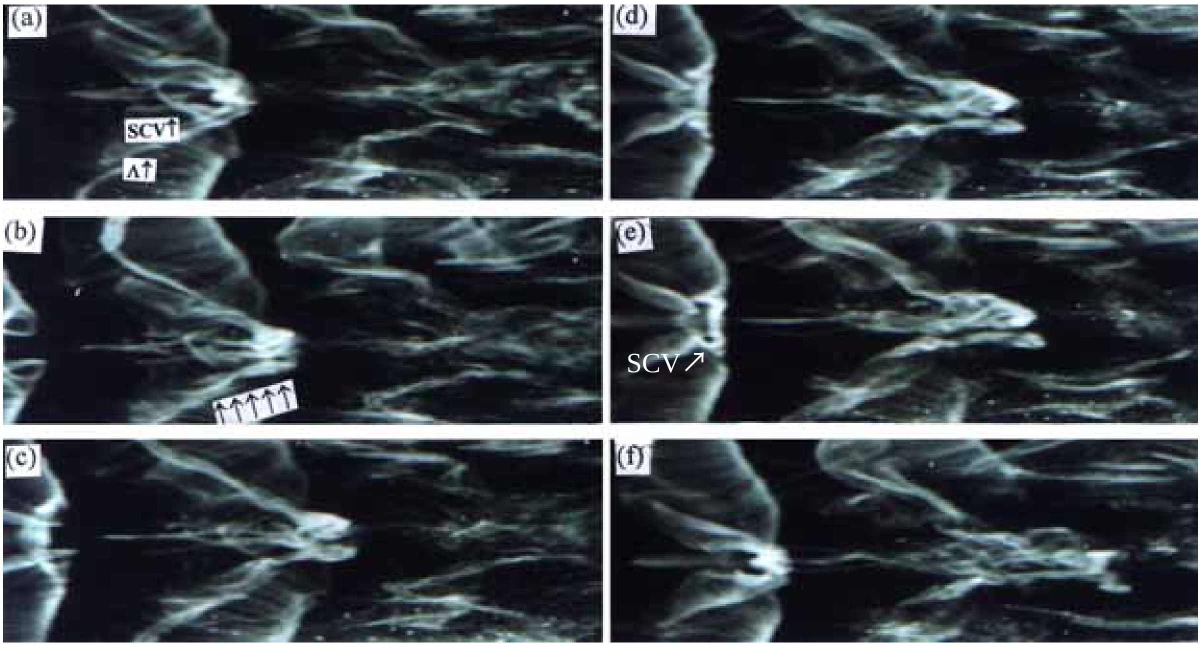

FIGURE 22. Formation of the streamwise vortices. (a) Start of interaction of the primary vortex and secondary closed vortices (SCV↑). (b)-(h) Filaments of both vortices are rolled up together (↑). (i)-(l) Axial instability of the vortex occurs as the interaction section breaks and the structure interacts with the other two connecting sections. The hydrogen bubble wire was at x = 350 mm and y = 1.5 mm. The time interval between successive pictures was 1/12 s. 1/2 scale from the actual of the photo sizes.

Figure 21 shows both the primary vortex called Λ-vortex and the secondary closed vortex. A long streak containing several CS-solitons appears in the very near-wall region. The middle layer has two real streamwise vortices which are the relatively long quasi-streamwise vortices (often counter-rotating pairs).

Figure 22 shows a sequence of photographs showing the interaction of a Λ-vortex and a secondary closed vortex.

In provide a clear understanding of the interaction, the leg of the Λ-vortex is divided into three sections: the upstream part, the interaction part and the downstream part. Attention here is focused on the interaction part. In general, the velocity fields of both vortices will cause their diameters to increase. Parts of the Λ-vortex filaments are induced into the secondary closed vortex, as discussed in the previous section. The other parts of the filaments of the Λ-vortex and the secondary closed vortex are rolled up together. The rolling velocity at their outer edge is much higher than that in the other two sections. Therefore, the structure will break at two points, one connecting the interaction section and the upstream section and the other connecting the downstream and interaction sections. The videos showed that these two bull horn-like vortices have higher rotation speed than in the other two sections. This process, reported here for the first time in a boundary layer flow, is a typical vortex axial instability.

Klebanoff et al. (1962) showed that streamwise vortices are generated from the three-dimensional development of the fundamental “peak-valley” spanwise structures. The present visual results show a new instability inducing the formation of the streamwise vortices.

9. Breakdown of the CS-solitons

Streaky structures elongated in the streamwise direction play a fundamental role in sustaining turbulence in wall-bounded shear flows (see, for examples, Kline et al. 1967, Kasagi 1988, Lian 1990), with much work done investigating the origin and breakdown of these structures in the turbulent regime. A theoretical analysis of the streak breakdown in channel flows was presented in recent papers on near wall turbulence by Nakagawa & Nezu (1981). In this model streak breakdown is one phase of a self-sustaining cycle in turbulent flow which includes streak formation, streak breakdown, and streamwise vortex regeneration from the nonlinear interaction of the streak instability eigenmode.

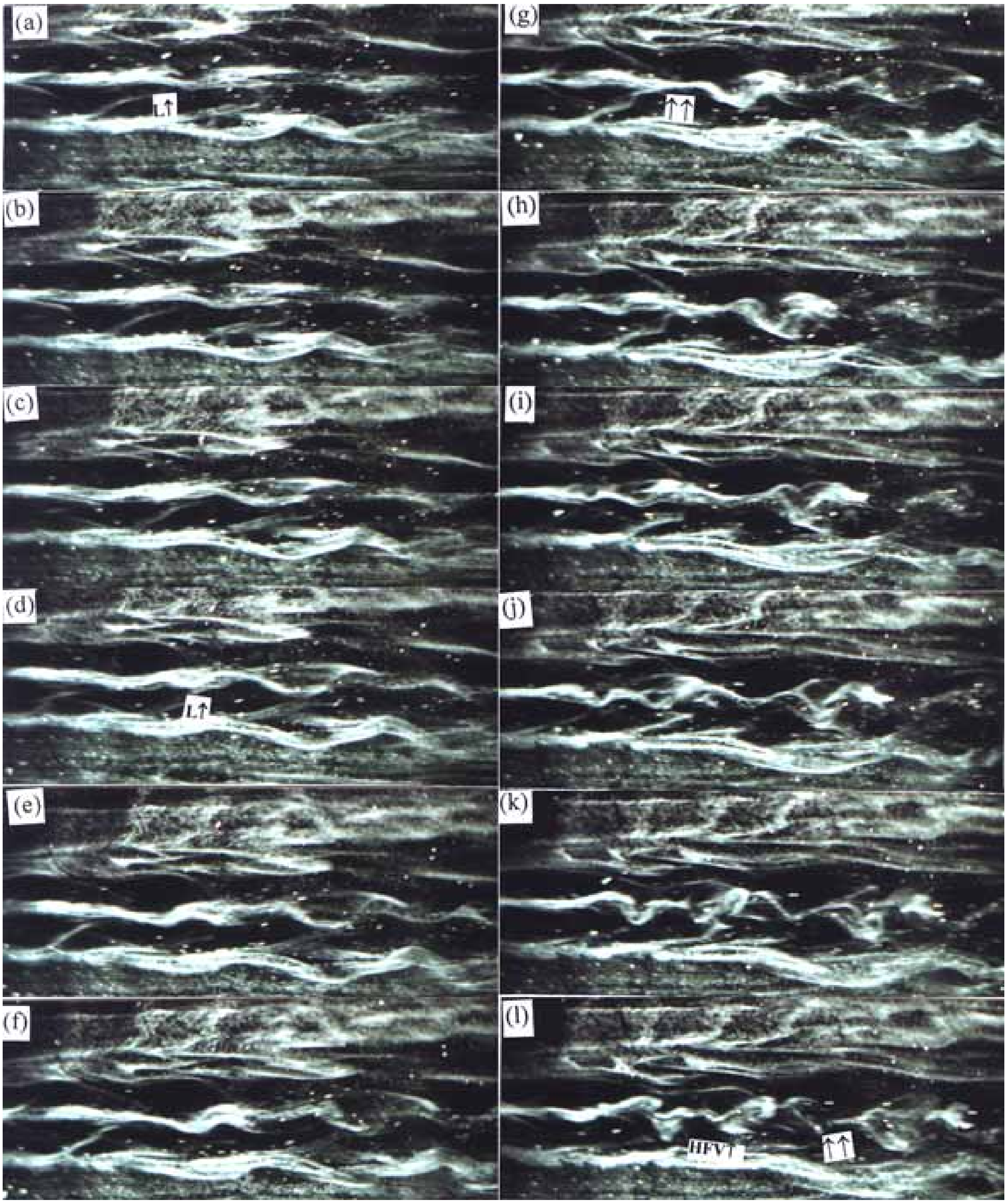

FIGURE 23. Breakdown of a long streak at x = 600 mm (L↑). (a)-(c) A regular long streak. (d)-(f) A wavy long streak. (g) Start of breakdown of a long streak. (h)-(l) Breakdown process associated with the appearance of the chain of ring vortices (HFV↑) in the “ peak position”. (l) The arrow points to the breakdown of the long streak. The hydrogen bubble wire was at x = 550 mm and y = 0.75 mm. The time interval between successive pictures was 1/12 s. 1/2 scale from the actual the photo sizes.

Figure 23 shows the regular breakdown of the long streak at x = 600 mm. A chain of ring vortices and the long streak can be seen. The chain of ring vortices was observed from their formation to the position of the long streak breakdown. Three stages of their formation and evolution were found (Lee 1998, 2000). First, they form along the borders of the CS-solitons and then separate from the CS-solitons one by one. Then, they meet the head of the Λ-vortex which increases their rotational speed. Because the convection velocity of the chain of ring like vortices is higher than that of the closed vortex, the chain of ring vortices separate from the Λ-vortex one by one. Next, the angle between the plane containing the vortices and the flat plate changes quickly to nearly 90^0 and the vortices propagate downstream at a speed of about 0.9 times the free stream velocity. They are visible even in the very late stage when the boundary layer becomes turbulence. They strongly affect not only the outer layer but also the near wall region.

Besides the main low frequency fluctuations, high amplitude fluctuations in the near-wall region which are generated by the CS-solitons as shown in figure 8 with additional spikes on the time traces generated by some of the chain of ring vortices. The breakdown occurs at x = 600 mm. An obvious relation between streak amplitude increase and the streak breakdown could not be found which is considered to be the necessary condition for streak breakdown suggested by Waleffe (1995, 1998).

The term breakdown used by Klebanoff et al. (1962) and other researchers describes what appears to be an abrupt change in the character of the wave motion at the peak. The breakdown process is characterized by intense fluctuations in the direction of the low velocity which occur for each cycle of the primary wave. The spatial extent of the initial breakdown as well as its physical significance can be determined by analyzing the manner in which the high frequency fluctuations characteristic of breakdown vary in the y and z directions. Although these characteristics are used to clearly define the breakdown, confusion often occurs. Our new definition for the breakdown of the Λ-vortex describes the formation of the high frequency vortices, i.e., the chain of ring vortices. The breakdown of the long streak describes the strong effects of the chain of ring vortices on the long streak with the harmonics found on the time traces in the near wall region.

10. Conclusion

A detailed flow structure have been presented describing the fluid dynamic processes in transitional boundary layer flows. The key element in the model is the CS-soliton, which is manifests the physics necessary to explain both the regeneration of vortices and the observed growth to larger scales farther from the wall. The CS-solitons are proposed to be the direct results of oblique wave interaction with the T-S waves catalyzing their formation based on the theory presented by Wu (1996) and Wu et al. (2001a,b).

The sequential process describing the interaction between the Λ-vortex and the secondary closed vortex, controls the manner in which the chain of ring vortices is periodically introduced from the wall region into the outer region of the boundary layer. There are several proposals to explain the generation of the high frequency vortices (Borodulin et al. 2002, Bake et al. 2002 and Lee 2000, 2001a,b) which is one of the key problems in understanding both transitional and developed turbulent boundary layers as well as other flows. The observation of the secondary closed vortex makes it possible to establish a real physical process for the formation of the high frequency vortices, i.e. the chain of ring vortices. The secondary closed vortex suggested here and the secondary hairpin vortex must be understood to explain the entire process. The present result suggests that the secondary hairpin vortex is just part of the closed vortex. If the secondary closed vortex is not considered, the dynamic processes and flow structures in a transitional boundary layer are very different from those in previous studies (Borodulin et al. 2002, Bake et al. 2002 and Lee 2000, 2001a,b). The present result also shows that both the breakdown of the chain of ring vortices and the breakdown of the long streak are periodic roughly, which was not been reported even in very recent studies by Bake et al. (2002).

The encouragement from Prof. S. Chen (Johns Hopkins University and Peking University) and Prof. M. D. Zhou (University of Arizona) is very helpful.

REFERENCES

ADRIAN, R. J., MEINHART, C. D. & TOMKINS, C. D. 2000 J. Fluid Mech. **422**, 1

BAKE, S., MEYER, D. G. W. & RIST, U. 2002 J. Fluid Mech. **459**, 217

BLACKWELDER, R. F. 1983 Phys. Fluids **26**, 2807

BORODULIN, V. I., GOPONENKO, V. R., KACHANOV, Y. S., MEYER, D. G. W., RIST, U., LIAN, Q. X. & LEE, C. B. 2002 Theoret. Comput. Fluid Dynamics **15**, 317

CANTWELL, B. J. 1986 J. Fluid Mech. **173**, 159

CLARK, J. A., MARKLAND, E. 1971 J. Hydr. Div. ASCE **97**, 1653

CRAIK, A. D. D. 1971 J. Fluid Mech. **50**, 393

CRAIK, A. D. D. 1985 Wave interactions and fluid flows, Cambridge Univ. Press

CROW, S. C. 1970 AIAA J. **8**, 2172

DOLIGALSKI, T. L.& WALKER, J. D. A. 1984 J. Fluid Mech. **139**, 1

ELDER, J. W. 1960 J. Fluid Mech. **9**, 235 .

EMMONS, H. W. 1951 J. Aeronant. Sci. **18**, 490

FALCO, R. E. 1977 Phys. Fluids Suppl., **20**, s124

FALCO, R. E. 1991 Phil. Trans. R. Soc. Lond. A **336**, 103

FASEL, H. & RIST, U. 1990 AIAA J. **28**, 29

FUKUNISHI, Y., SATO, H & INOUS, O. AIAA paper. No. 87-1253 (1987).

GASTER, M. & GRANT, T. 1975 Proc. R. Soc. London A **347**, 253

HAMA, F. R., LONG, J. D. & HEGARTY, J. C. 1957 J. Appl. Phys., **28**, 388.

HAMA, F. R. & NAUTANT, J. 1963 In Proc. of Heat Transfer & Fluid Mech. Inst.pp.77-93. Stanford Univ. Press

HINZE, J. O. 1975 Turbulence, McGraw-Hill Company, New York

JOSLIN, R. D., STREET, C. R.& CHANG, C. L. 1993 Theor. Comput. Fluid Dyn. **4**, 171

KASAGI, N. 1988, In Near Wall Turbulence: Zaric Memorial Conf. (eds. Kline, S. J. and Afgan, N. H.), Hemisphere, New York

KACHNAOV, Y. S. 1994 Annu. Rev. Fluid Mech. **26**, 411

KACHANOV, Y. S. & LEVCHENKO, V. Y. 1984 J. Fluid Mech. **138**, 209

KACHANOV, Y. S., KOZNOV, V. V. & LEVCHENKO, V. Y. 1974a Izv. Sib. Otd. Akad. Nauk SSSR, Ser. Tekh. Nauk **13**, 2

KACHANOV, Y. S., KOZNOV, V. V. & LEVCHENKO, V. Y. 1974b Izv. Sib. Otd. Akad. Nauk SSSR, Ser. Tekh. Nauk **13**, 18

KIM, H. T., KLINE, S. J. & REYNOLDS, W. C. 1971 J. Fluid Mech. **50**, 133

KLEBANOFF, P. S., TIDSTROM, K. D. 1959 NACA Tech. Note D-195

KLEBANOFF, P. S., TIDSTROM, K. D. & SARGENT, L. M. 1962 J. Fluid Mech. **12**, 1

KLINE, S. J., REYNOLDS, W. C., SCHRAUB, F. A. & RUNSTALLER, W. P. 1967 J. Fluid Mech. **30**, 741

KNAPP, C. R. & ROACHE, P. J. 1968 AIAA J. **6**, 29

KOKSHAYSKY, N. V. 1979 Nature **279**,176; MOORE, D. W. & SAFFMAN, P. G. 1972 Phil. Trans. Roy. Soc. London A. **272**, 403

KOVASZNAY, L. S., KOMODA, H. & VASUDEVA, B. R. 1962 in Proc. of Heat Transfer & Fluid Mech. Inst. pp. 1-26. Stanford Univ. Press

LEE, C. B. 1998 Phys. Letts A **247**, 397

LEE, C. B. 2000 Phys. Rev. E**62,** 3659

LEE, C. B. 2001a Exps. In Fluids, **30**, 354

LEE, C. B., 2001 In Proc. of Heat Transfer & Fluid Mech. Inst. pp.61-80. California State University Press

LIAN, Q. X. 1990 J. Fluid Mech. **215**, 101

LOEHRKE, R. I. & MORKOVIN, M. B. 1975 J. Fluid Eng., Trans ASME **97**, 534

MANGUR, C. J. 1977 AIAA Pap. No. 77-1369

MELANDER, M. V.& Zabuski, N. J. 1988 Fluid Dynamics Res. **3**, 247

MELANDER, M. V. & HUSSAIN, F. 1989 Phys. Fluids A **1**, 633

MITCHNER, M. J. 1954 J. Aeronaut. Sci. **29**,440

MOIN, P., LEONARD, A. & KIM, J. 1986 Phys. Fluids **29**, 954

MORKOVIN, M. V. 1969 AFFDL-TR- 68-49

NAKAGAWA, H. NEZU,1981 J. Fluid Mech. **104**, 1

NISHIOKA, M., ASAI, M. & IIDA, S. 1990 In Proc. of International Union of Theoretical and Applied Mechanics on Laminar-Turbulent Transition, Springer

REDDY, S. C., SCHMID, P. J., BAGGETT, J. S. & HENNINGSON, D. S.1998 J. Fluid Mech. **365**, 269

RIST, U. & FASEL, H. 1995 J. Fluid Mech. **298**, 211

ROBINSON, S. K. 1990 AIAA paper No.90-1638

ROBINSON, S. K. 1991 Annu. Rev Fluid Fluid **23**, 601

ROBINSON, S. K. 1991 NASA Tech. Memo. 103859

ROGLER, H. L. 1977 AGARD-CP-244, Pap. No. 14

ROGLER, H. L.& RESHOTKO, E. 1975 SIAM J. Appl. Mech. **28**, 431

ROTT, W. 1956 Q. Apply Math **13**, 444

SAFFMAN, P. G. 1990 J. Fluid Mech. **212**, 395

SAPIRO, P. J. 1977 MIT Acoustic and Vibration Lab. Rep. 83458-83560-1

SARIC, W. S., REED, H. L.& KERSCHEN, F. J. 2002 Annu. Rev. Fluid Mech. **34**, 291

SEARS, W. R. 1956 J. Aero. Sci. **23**, 490

SCHLICHTING, H. 1979 Boundary layer theory, McGraw-Hill, New York

SCHUBAUER, G. B. 1957 Boundary Layer Research, Springer-Verlag

SCHUBAUER, G. B. & KLEBANOFF, P. S. 1956 NACA Rep. 1289

SMITH, C. R.& SCHWARTZ, S. P. 1983 Phys Fluids **26**, 641

SMITH, C. R., WALKER, J. D. A., HAIDARI, A. H. & SOBRUN, U 1991 Phil. Trans. R. Soc. London A**336**,131

THEFETHEN, L. N., THEFETHEN, A. E., REDDY, S. C. & DRISCOLL, T. A. 1993 Science **261**,578

THEODORSEN, T. 1952 Proc. 2nd Midwestern Conf. On Fluid Mech. Ohio State University

THOMAS, A. S. W. & SARIC, W. S. 1981 Bull. Am. Phys. Soc. **26**,1252

VASUDEVA, B. R. 1967 J. Fluid Mech., **29**, 749

WALEFFE, F. 1995 Phys Fluids, **9**, 883

WALEFFE, F. 1998 Phys Rev Letts., **81**, 4140

WALKER, J. D. A., ABBOTT, D. E., SCHARNHORST, R. K. & WEIGAND, G. G. 1989 AIAA J. **17**, 140

WILLIAMS, D. R., FASEL, H. & HAMA, F. R. 1984 J. Fluid Mech. **149**,179

WU, X. 1996 J. Fluid Mech., **397**, 285

WU, X. & LU, J.2001 Annual research Briefs of Center for Turbulence Research at Stanford University, Stanford University;

WU, X. & CHOUDHARI, M. 2001 Annual Research Briefs of Center for Turbulence Research at Stanford University, Stanford University

ZAWADZKI, I. & AREF, H. 1991 Phys. Fluids A **3**, 1405